

EdSr: A Novel End-to-End Approach for State-Space Sampling in Molecular Dynamics Simulation

Hai-Ming Cao¹, Bin Li^{1*}

December 31, 2024

Abstract

The molecular dynamics (MD) simulation technique has been widely used in complex systems, but the time scale is limited due to the small timestep. Here, we propose a novel method, named Exploratory dynamics Sampling with recursion (EdSr), which is inspired by Langevin dynamics, Stochastic Differential Equation and Taylor expansion formula, can be used in MD simulation with flexible timestep. By setting up four groups of experiments including simple function, ideal physical model, all-atom simulation and coarse-grained simulation, we demonstrate that EdSr can dynamically and flexibly adjust the simulation timestep according to requirements during simulation period, and can work with larger timestep than the widely used velocity-Verlet integrator. Although this method can not perform perfectly at flexible timestep with all simulation systems, we believe that it will be a promising approach in the future.

Introduction

The molecular dynamics (MD) simulation method, a branch of multiscale modeling architecture, has been widely used in many research areas, such as soft matter, chemical engineering, material science and biological system. The MD simulation method is based on Newton's second law of motion and statistical mechanics, and it was firstly developed at 1950s [1]. Nowadays, the efficiency and accuracy of MD simulations have been improved significantly due to the enhancement of computer hardware and algorithms. There are a series of MD simulation techniques due to the different time and lengths scales [2, 3]. For instance, the all-atom (AA) MD simulation is used to simulate evolution of complicate systems with a relatively high precision [4, 5, 6]; and the coarse-grained (CG) simulation method, which treats several atoms or molecules into a single CG bead, is able to capture the global behavior of macromolecules with a less computational cost and an acceptable bias [7, 8, 9, 10, 11, 12].

Although MD simulations exhibit many advantages, like the investigation of underlying mechanism in experimental phenomenons, prediction for future material designs, and so on, the computation of complex interactions, the limitation of timestep Δt , as well as other factors result in highly computational cost in MD simulations. Some researchers have proposed lots of methods to try to overcome the computational cost by fitting force field, such as Machine learning Force Field [13, 14, 15]. However, the integration timestep still limits the time scale of MD simulation. Some of the classical time integration algorithms, such as velocity-Verlet integrator [16], predictor-corrector [17], leap frog integrator, multi-stepping time integrator [18], have been practically implemented to solve evolution of complicated molecular systems in some conventional simulation software, like LAMMPS [19], GROMACS [20, 21], etc. On the other hand, some methods like Physics-Informed Neural Networks (PINN) [22, 23, 24, 25], combining machine learning and physical mechanics, have been proposed for solving ordinary differential equation (ODE) with respect to evolution of dynamical systems. Recently, with the development of machine learning, as well as the success of score-based model based on Langevin dynamics [26] and Denoising Diffusion Probabilistic Model (DDPM) [27, 28] in the field of Computer Vision (CV), researchers tried to adopt these methods for enlarging timestep and have proposed a series of methods on the basis of diffusion model. For example, Wu et al. proposed an equivariant geometric transformer based on diffusion process to sample atomic positions [29], Schreiner et al. proposed an Implicit Transfer Operator (ITO) for building multiple time-scale surrogate models [30], Hsu and co-workers adopted score dynamics to accelerate the evolution of systems of MD simulations [31].

The aforementioned methods have been able to sample state of ensembles at larger timestep by predicting probability density distribution, there are still some issues to be solved. Firstly, it is inflexible to adjust the timestep, as these methods only sample

¹School of Chemical Engineering and Technology, Sun Yat-Sen University, Zhuhai 519082, China. E-mail: libin76@mail.sysu.edu.cn

positions of the same time interval Δt as training. On the other hand, some of these methods need tens of thousands of data to train the machine learning model. To solve these problems, we propose a novel algorithm based on Taylor expansion and Langevin dynamics, so-called **Exploratory dynamics Sampling with recursion (EdSr)**. By using a recursive divergence process, our method can dynamically and flexibly adjust the simulation timestep according to requirements during simulation period without the way of data-driven.

In order to test the performance and accuracy of the EdSr method, we conduct comprehensive experiments on some simple functions, ideal physical models [24], atomistic simulations [5], and coarse-grained simulations [32, 33, 34]. By comparing with velocity-Verlet (VV) integrator (one of the most used methods in MD simulations), the EdSr method not only performs higher precision at the same timestep, but also is able to hold on at least two times (relying on complexity of explicit ensemble) larger timestep than VV with an acceptable bias. At the same time, we also test negative integration timestep for ideal physical models, to validate the time reversible symmetry of EdSr method. The results show that the EdSr method has a high precision for the ability of time reversible symmetry.

Results

The algorithm of EdSr is introduced in **Methods**. In order to test the performance of the EdSr method, we conduct comprehensive experiments which are from simplicity to complication: simple functions, ideal physical models, all-atom MD simulation and coarse-grained MD simulation.

Simple Function

We design two groups of sub-experiments for simple function tests, in order to investigate the influence of the interval Δx of EdSr, and the performance of constructing function by EdSr. The first one is that the functions are constructed with a fixed initial point x_0 as a hyper-parameter and a variable interval Δx . The other one is that the functions are constructed with both initial point x_0 and interval Δx as two fixed hyper-parameters.

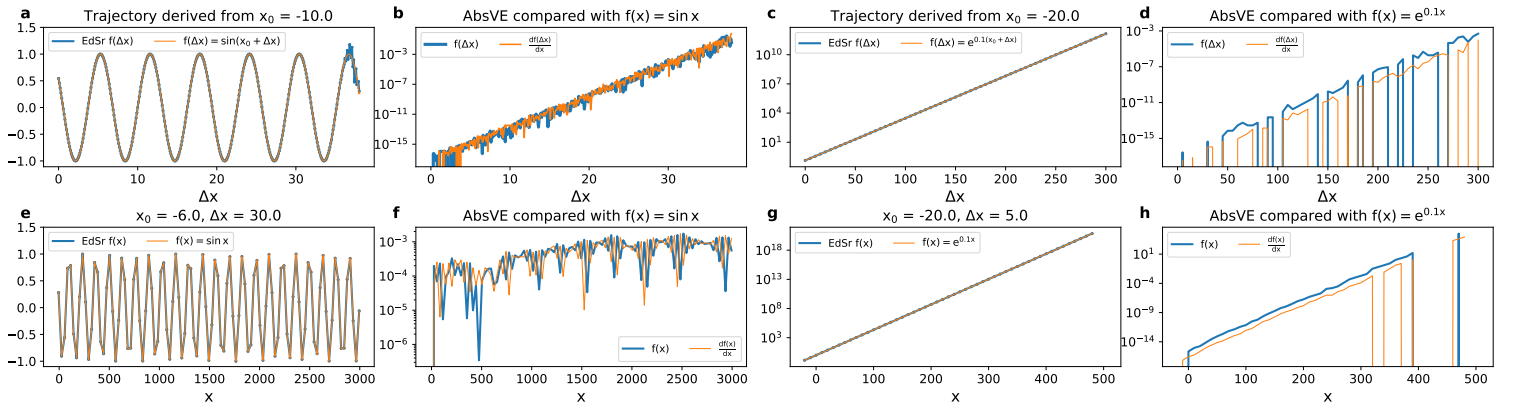


Fig. 1: Results of the two groups of sub-experiments of simple functions. (a-d) show the results of the first group of sub-experiments, including the trajectories versus Δx , as well as the AbsVEs compared with source functions; (e-h) show the results of the second group of sub-experiments. (a),(b),(e),(f) show the results of $f(x) = \sin x$; (c),(d),(g),(h) show the results of $f(x) = e^{0.1x}$;

Fig. 1a and c show comparisons between the two source functions ($f(x) = \sin x$ and $f(x) = e^{0.1x}$) and the results constructed by EdSr with variable intervals Δx . We observe excellent consistency between the source function of $f(x) = \sin x$ and the result of EdSr, the obvious deviation does not appear until the interval Δx is greater than 35.0 (Fig. 1a). The results of $f(x) = e^{0.1x}$ obtained via EdSr approach do not show evident deviation through all the intervals (Δx) we investigate (Fig. 1c). We also compute the absolute value of error (AbsVE) of $f(x)$ and the corresponding derivative between EdSr and source function, which are shown in Fig. 1b and d. We find that AbsVE increases as the interval Δx increases. However, the scales of AbsVE shown in Fig. 1b and d indicate that EdSr can hold on a relatively high precision across different intervals.

In the second group of sub-experiments, we fix both initial point x_0 and interval Δx and use the way of which $f(x_0 + n * \Delta x)$ derives from $f(x_0 + (n - 1) * \Delta x)$ to construct functions. The comparisons between the results of EdSr and source function, as well as the AbsVEs and their corresponding derivatives are shown in Fig. 1e-h. EdSr is also able to hold on a high precision in a long series, by comparing with source functions and the corresponding derivatives. Note that as shown in Fig. 1h, although both

the AbsVE results of functions and derivatives are over 10^1 , it is negligible compared with the scale of the source function values (Fig. 1g). We also test some other functions like $f(x) = x^2 - 2x - 5$, $f(x) = \text{sigmoid}(x)$ and $f(x) = x^3$. The comparisons between the results obtained via EdSr and the source functions are shown from Fig. S1 to Fig. S4 in **Supplementary Information**.

Ideal Physical Models

In this part, we refer to some ideal physical models, including ideal spring model, ideal pendulum model and two-body model, which were also studied in Hamiltonian Neural Networks (HNN)[24], and adopt them to verify the performance of EdSr. We also design the same two groups of sub-experiments, including a fixed initial time t_0 and a variable interval Δt , as well as both fixed t_0 and interval Δt , identical setting as in simple functions respectively. In order to check the time reversible symmetry of EdSr method on the ideal physical models, we set two series of Δt values, including positive Δt and negative Δt . Besides, we use Runge-Kutta method of order 5(4) (RK45)[35] and smaller step size to generate trajectory data as ground truth (GT), the data generated by velocity-Verlet integrator (VV) are set as control group.

Ideal Spring

First, we adopt the ideal spring model to test the performance of EdSr, in which the Hamiltonian is described as the following equation:

$$\mathcal{H} = \frac{1}{2}kq^2 + \frac{1}{2}mv^2 \quad (1)$$

where k is the spring constant, q is the generalized coordinate, and m is the mass, v is the velocity. Here, we set $k = m = 1$ for simplicity.

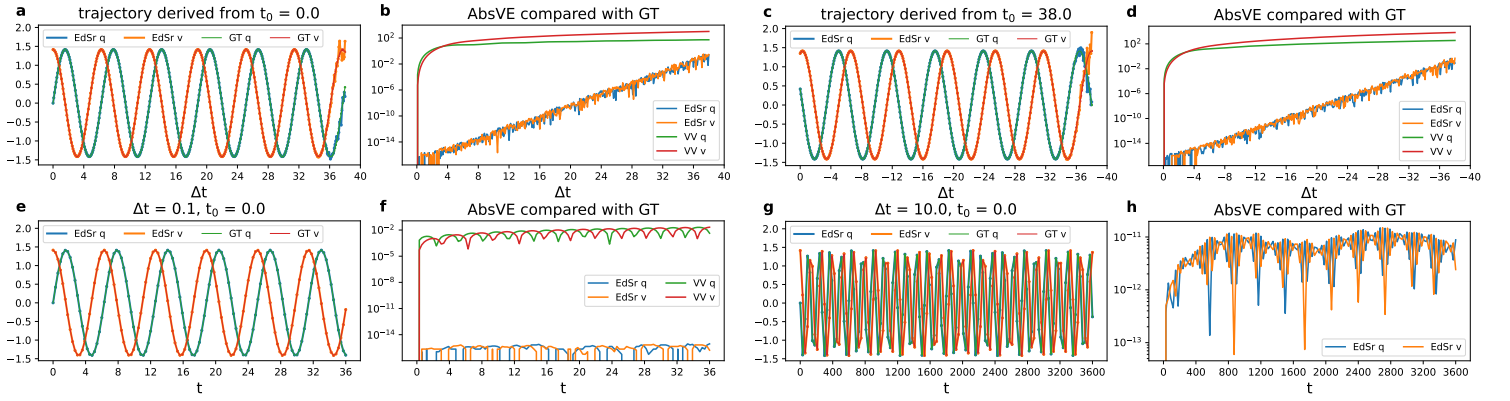


Fig. 2: Results of two groups of sub-experiments of ideal spring. (a-d) show the results of the first group of sub-experiments, and (e-h) show the results of the second group of sub-experiments. (a) Blue line, orange line denote generalized coordinates q , velocities v generated by EdSr with positive Δt , respectively. Green line, red line denote q and v obtained in GT, respectively. (b) Blue line, orange line denote AbsVEs between EdSr and GT. Green line, red line denote AbsVEs between VV and GT. (c), (d) are same as (a), (b), but with negative Δt . (e), (f) show the comparisons of q and v between EdSr and GT, and the corresponding AbsVEs with $\Delta t = 0.1$. (g), (h) denote the results with $\Delta t = 10.0$, the corresponding AbsVEs between VV and GT are not shown as they are very huge (over 1×10^2).

Similar to simple functions, we design the same two groups of sub-experiments on ideal spring (Fig. 2). In the first group of sub-experiments, we show the variations of coordinates and the corresponding velocities over Δt , as well as AbsVEs of EdSr and VV compared with GT (Fig. 2a and b). For verification on time-reversal symmetry, we also perform the tests backwards by setting negative Δt (Fig. 2c and d). EdSr exhibits much higher precision than VV integrator at same Δt value by comparing with GT. The obvious deviation does not appear until Δt is greater than 35 for EdSr method. Moreover, EdSr is able to hold on negative Δt , from the comparisons between Fig. 2a and c, as well as Fig. 2b and d, indicating that EdSr shows excellent performance for the systems with time symmetrical property. In the second group of sub-experiments, we generate the trajectories of ideal spring at $\Delta t = 0.1$ and 10.0 , respectively (Fig. 2e-h). Both the coordinates and velocities generated by EdSr are very close to those from GT at small timestep $\Delta t = 0.1$ and large timestep $\Delta t = 10.0$ (Fig. 2e and g), and the AbsVEs are much smaller at the two selected Δt values than VV integrator (Fig. 2f and h). Thus, it is unquestionable that EdSr shows the better performance on the ideal spring model than VV. We also perform the second group of sub-experiments by setting $\Delta t = 1.0$ and 5.0 , and the results are provided in Fig. S5.

Ideal Pendulum

The Hamiltonian of ideal pendulum without friction can be described as:

$$\mathcal{H} = mgl(1 - \cos \theta) + \frac{1}{2}ml^2v^2 \quad (2)$$

where m , g , l , θ and v are the mass of pendulum, gravitational constant, length of pendulum, angle and angular velocity respectively. To simplify the experiment, we set $m = l = 1$, and $g = 4$. The angle θ and angular velocity v are initially set to $\frac{\pi}{3}$ and 0, respectively.

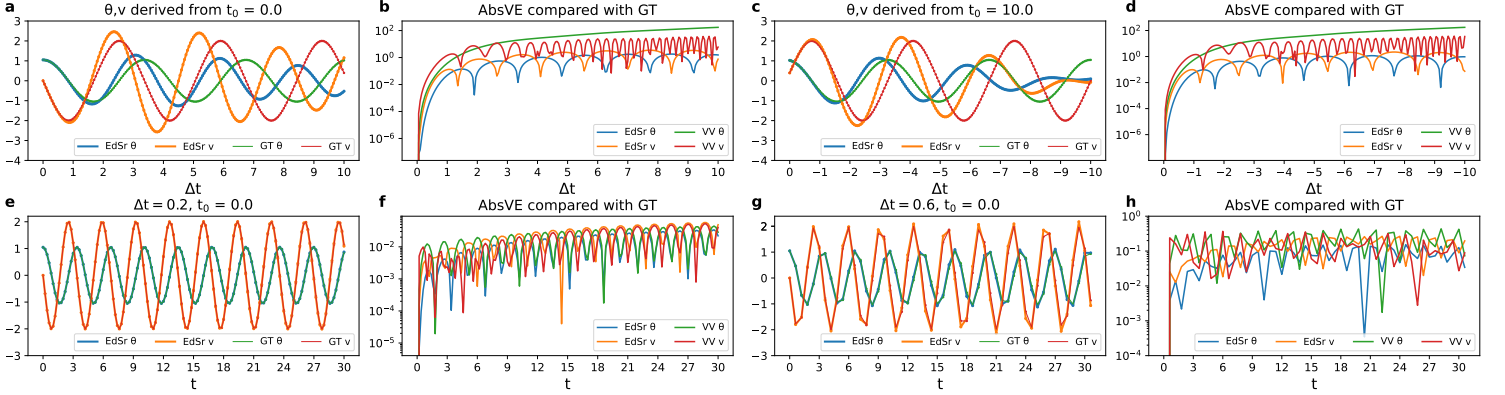


Fig. 3: Results of two groups of sub-experiments of ideal pendulum. (a-d) show the results of the first group of sub-experiments, and (e-h) show the results of the second group of sub-experiments. (a) Blue line, orange line denote angles θ , angular velocities v generated by EdSr with positive Δt , respectively. Green line, red line denotes angles θ , angular velocities v generated by GT, respectively. (b) Blue line, orange line denote AbsVEs between EdSr and GT; green line, red line denote AbsVEs between VV and GT. (c) and (d) are same as (a) and (b), respectively, but with negative Δt . (e),(f) show the comparisons of θ and v between EdSr and GT, and the corresponding AbsVEs with $\Delta t = 0.2$. (g),(h) denote the results with $\Delta t = 0.6$.

In the first group of sub-experiments, Fig. 3a shows the results of angles θ and angular velocities v over positive Δt values obtained through EdSr method and the comparison with GT, and the reverse time evolutions (negative Δt) of θ and v are exhibited in Fig. 3c. The results of θ and v obtained via EdSr are close with those from GT, but the deviations become larger as the increase of absolute Δt . We also investigate the AbsVEs of EdSr compared with GT, together with those from VV integrator (Fig. 3b and d). Although AbsVE values grow with the increase of absolute Δt for both EdSr and VV, the AbsVEs of θ and v generated by EdSr are smaller than those obtained via VV integrator. The results shown in Fig. 3a-d also indicate that EdSr is time symmetrical. Fig. 3e-h shows the results of the second group of sub-experiment with $\Delta t = 0.2$ and 0.6 . EdSr shows smaller deviation than VV integrator on making a long time simulation with the selective Δt values. The results with absolute $\Delta t = 1.0$ for the ideal pendulum are shown in Fig. S6, which exhibit that EdSr and VV have similar results.

Two-Body Model

In the two-body model, one particle interacts with the other particle by Law of universal gravitation. Therefore, the Hamiltonian for two-body system can be described as:

$$\mathcal{H} = \frac{1}{2}(m_1 + m_2)V^2 + \frac{1}{2}\mu(v_1^2 + v_2^2) + G \frac{m_1 m_2}{|q_1 - q_2|} \quad (3)$$

where m_1 , q_1 , v_1 are mass, coordinates, velocity of one particle, respectively; while m_2 , q_2 , v_2 are the counterparts. G is the universal gravitational constant, μ is the reduced mass and V is the velocity of center of mass. For simplicity, we set $G = m_1 = m_2 = 1$, $V = 0$.

In the first group of sub-experiments of two-body model, we also firstly test the performance of EdSr on both positive Δt and negative Δt . As shown in Fig. 4, we visualize the trajectories of particles (Fig. 4a and d), and calculate thermodynamic properties including total energies (E_{Tot}), kinetic energies (E_{Kin}) and potential energies (E_{Pot}) (Fig. 4b and e). The trajectories of particles and different energies obtained through EdSr are close with GT if $\Delta t < 2.0$, then the deviations are observed for these properties. For the comparison of calculated position q and velocity v with VV integrator, we compute the Mean Absolute Error (MAE, Equation (4)) between EdSr and GT, as well as between VV and GT, respectively. The MAE is calculated as:

$$\text{MAE} = \frac{1}{4} \sum_{i=1}^{N:2} \sum_{j=1}^{ndim:2} |X_{ij} - \text{GT}_{ij}| \quad (4)$$

where $N = 2$ means the particle number in the two-body model, $ndim = 2$ indicates the two-dimensional system, X denotes the outputs from EdSr or VV group. The results of MAEs generated from EdSr and VV by comparing with GT are exhibited in Fig.

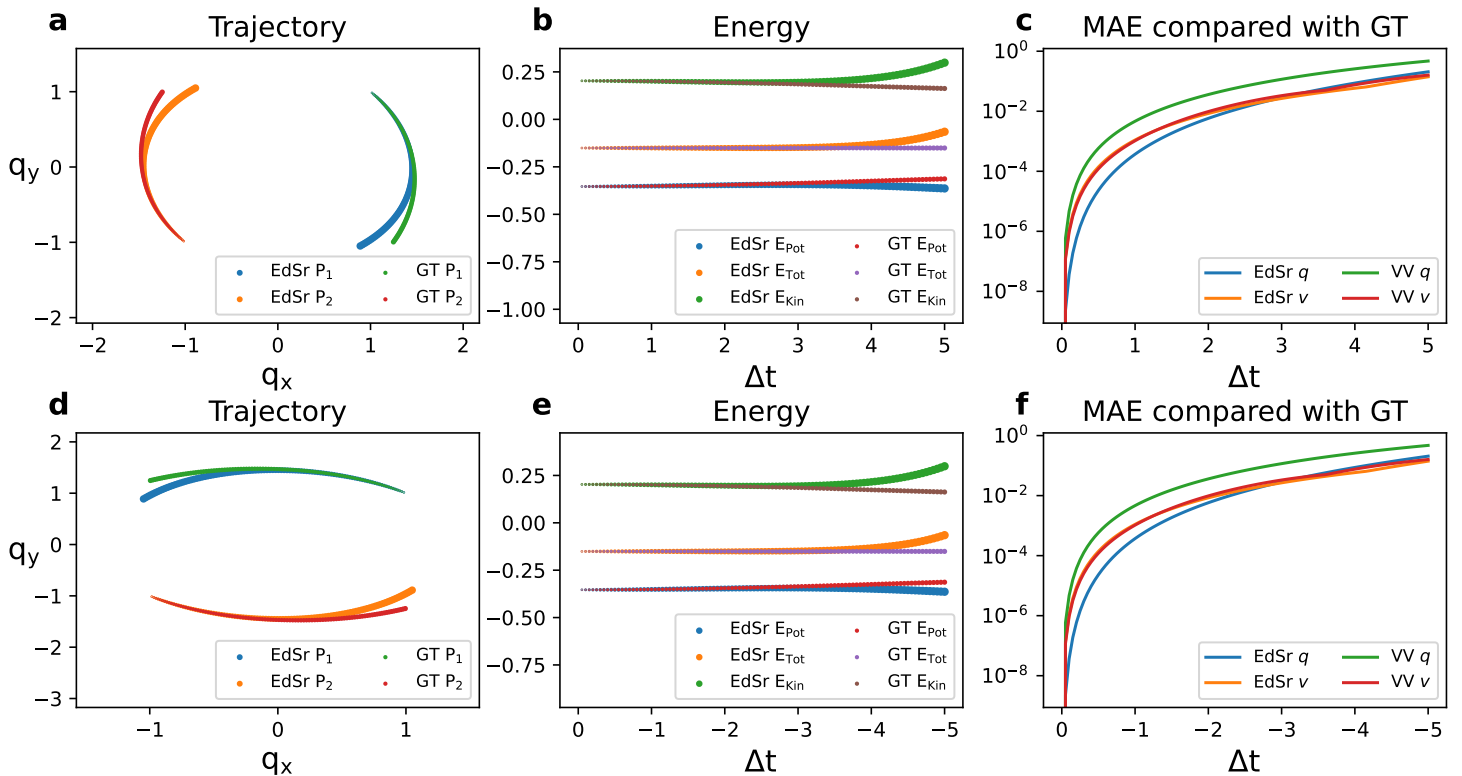


Fig. 4: Results of the first group of sub-experiment of two-body model. (a), (d) denote the positions of the particles in two-body (P_1 and P_2) generated by EdSr and GT, the symbol sizes increase as the absolute Δt values vary from 0.0 to 5.0. (b), (e) exhibit kinetic energies (E_{Kin} , green line and brown line), total energies (E_{Tot} , orange line and purple line), potential energies (E_{Pot} , red line and blue line) from EdSr and GT over Δt . (c), (f) denote the MAEs between EdSr and GT (blue and orange lines), and compare with that between VV and GT (green and red lines) over Δt .

4c and f, at positive Δt and negative Δt values, respectively. Basically, the deviation of position q appears when the absolute Δt is greater than 2.0 for both EdSr and VV integrator. However, the MAE of position q obtained via EdSr is obviously lower than VV integrator, indicating the higher accuracy of EdSr method. The MAE of velocity v generated via EdSr and VV integrator are close with each other.

In the second group of sub-experiments of two-body model, we generate just one period of data for the Δt values which we set up, in order to compare the performance of EdSr with GT and VV strictly. Here we mainly show the results of $\Delta t = 0.5$ and $\Delta t = 1.0$ in Fig. 5. The overall trajectories of two particles obtained via EdSr is similar as those of GT (Fig. 5a and d), except that “a forward effect” appears in EdSr, that is, it seems to be a little “faster” than GT. “The forward effect” becomes more obvious as the increase of Δt . The time evolutions of potential energy, total energy and kinetic energy of EdSr are very close to those of GT at both $\Delta t = 0.5$ and 1.0 (Fig. 5b and e). EdSr shows higher accuracy of q and v than VV integrator in short-time simulation ($t < 21.0$), through the MAE results compared with GT (Fig. 5c and f). But the performance of EdSr is similar as VV integrator if the simulation time $t > 21.0$. We also examine the results generated by EdSr at negative Δt with identical absolute values (Fig. S7), which show the same behavior as Fig. 5. The results of second group of sub-experiments of two-body model with at Δt values are shown in Fig. S8.

All-Atom MD Simulation

Here, in order to test the application of EdSr method in MD simulation, we adopt our previous work of diffusion of indole in beta zeolite, namely *indole@Beta zeolite*, as the all-atom MD simulation test system [5]. We use LAMMPS software to run the simulations. The core-shell force field [36, 37, 38] and interface force field [39, 40] are adopted to optimize the zeolite structure and perform the MD simulation for zeolite, respectively, the OPLS force field is used for indole molecule. The detailed system information is available in our previous paper [5]. Firstly, we perform 1.0 ns simulation in the canonical ensemble (NVT), with the temperature at 700 K controlled by Nosé-Hoover thermostat[41, 42], in order to make the system achieve thermodynamical equilibrium. Afterwards, we use VV integrator implemented in LAMMPS and small timestep $\Delta t = 0.01$ fs as the benchmark group (**BM group**), use VV integrator and larger timesteps $\Delta t = 1.0, 2.0, 3.0$ fs as control group (**MD group**), $\Delta t = 3.0$ fs is the largest timestep we can perform the simulation for the system with VV integrator. We use EdSr at the timesteps $\Delta t = 1.0, 2.0, 3.0, 4.0$ fs to run the simulations (**EdSr group**). The MD and EdSr groups are run under micro-canonical ensemble (NVE)

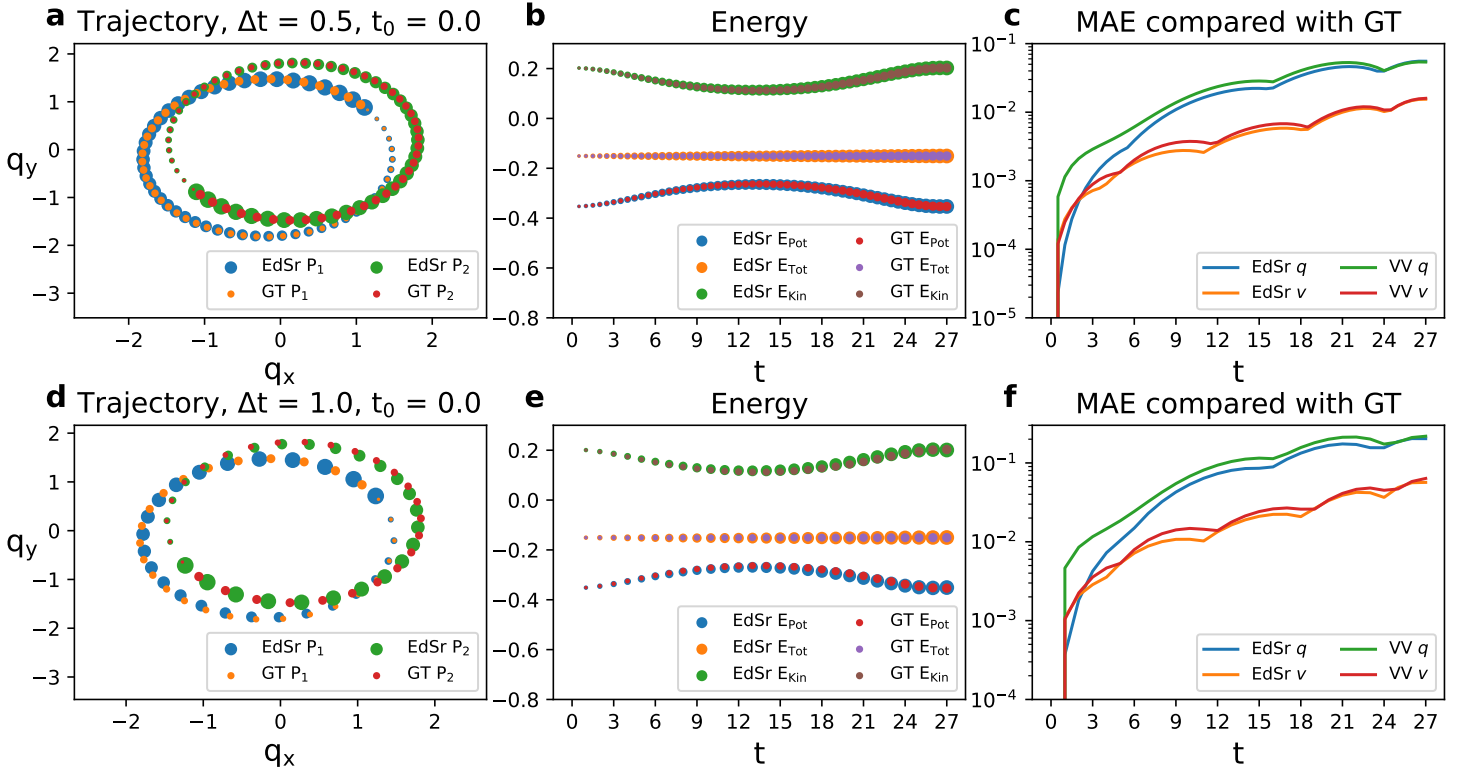


Fig. 5: Results of the second group of sub-experiments of two-body model. (a),(d) denote the time evolutions of positions of the particles in two-body (P_1 and P_2) generated by EdSr and GT, the symbol sizes increase as the time starts from 0.0 to 27.0. The time evolutions of different energies obtained by EdSr and GT are exhibited in (b), (e). (c),(f) denote the MAEs between EdSr and GT, and compare with those between VV and GT over simulation time.

with 1×10^4 steps, and the BM group is performed for the same simulation time as MD and EdSr groups at NVE ensemble. So far, as we have not yet embedded EdSr into LAMMPS software, we only take LAMMPS software as “force engine” and use Python script to run EdSr. However, unlike the EdSr, BM and MD groups use LAMMPS and their own “run” API to run simulations. Here, we also calculate the MAE for characterizing the performance of EdSr and MD groups, which is redefined as:

$$\text{MAE} = \begin{cases} \frac{1}{N * M} \sum_{i=1}^{N:\text{atoms}} \sum_{j=1}^{M:\text{ndims}} |X_{ij} - \text{BM}_{ij}| & \text{(a)} \\ \frac{1}{N} \sum_{i=1}^{N:\text{time}} |X_i - \text{BM}_i| & \text{(b)} \end{cases} \quad (5)$$

where X denotes the outputs from EdSr or MD group. We use Equation 5a to compute MAE of three dimensional ($ndims = 3$) coordinates, and Equation 5b to compute MAEs of some scalar properties like energy, root mean square deviations (RMSD), and so on.

First, we randomly select one representative indole molecule in the system, and compare the MAEs of the indole molecule coordinates between EdSr and BM groups, as well as between MD and BM groups. The MAE obtained via EdSr versus BM is smaller than MD at $t < 6$ ps at $\Delta t = 1.0$ fs (Fig. 6a), then the two methods generate similar results at longer time. On the other hand, the MAE from EdSr method is obviously smaller than MD at $\Delta t = 3.0$ fs (Fig. 6c), indicating the higher accuracy of EdSr for generating trajectory at larger timestep, which could be also observed from the averaged MAEs from the comparisons between EdSr and MD (dashed lines in Fig. 6a and c). Thus, EdSr performs better than MD group on building trajectory of indole molecules. The RMSDs from BM, MD and EdSr groups at $\Delta t = 1.0$ and 3.0 fs are shown in Fig. 6b and d, respectively. The RMSD results also exhibit that the MD and EdSr groups are similar with each other at smaller timestep of 1.0 fs, and EdSr performs better than MD at larger timestep of 3.0 fs.

In order to test the performance of EdSr more comprehensively, we compare thermodynamics features by computing the time evolutions of total kinetic energy, total non-bonded pairwise energy, and intramolecular energy of indoles (Fig. 7), and then we also compute the MAEs of different energies between EdSr and BM groups, as well as MD and BM groups (insets in Fig. 7). Generally speaking, it is clear that, the EdSr method shows smaller deviation than VV integrator in all thermodynamic features at both $\Delta t = 1.0$ fs (Fig. 7a-c) and $\Delta t = 3.0$ fs (Fig. 7d-f) for the system. Especially if $\Delta t = 3.0$ fs, the MAE of intramolecular

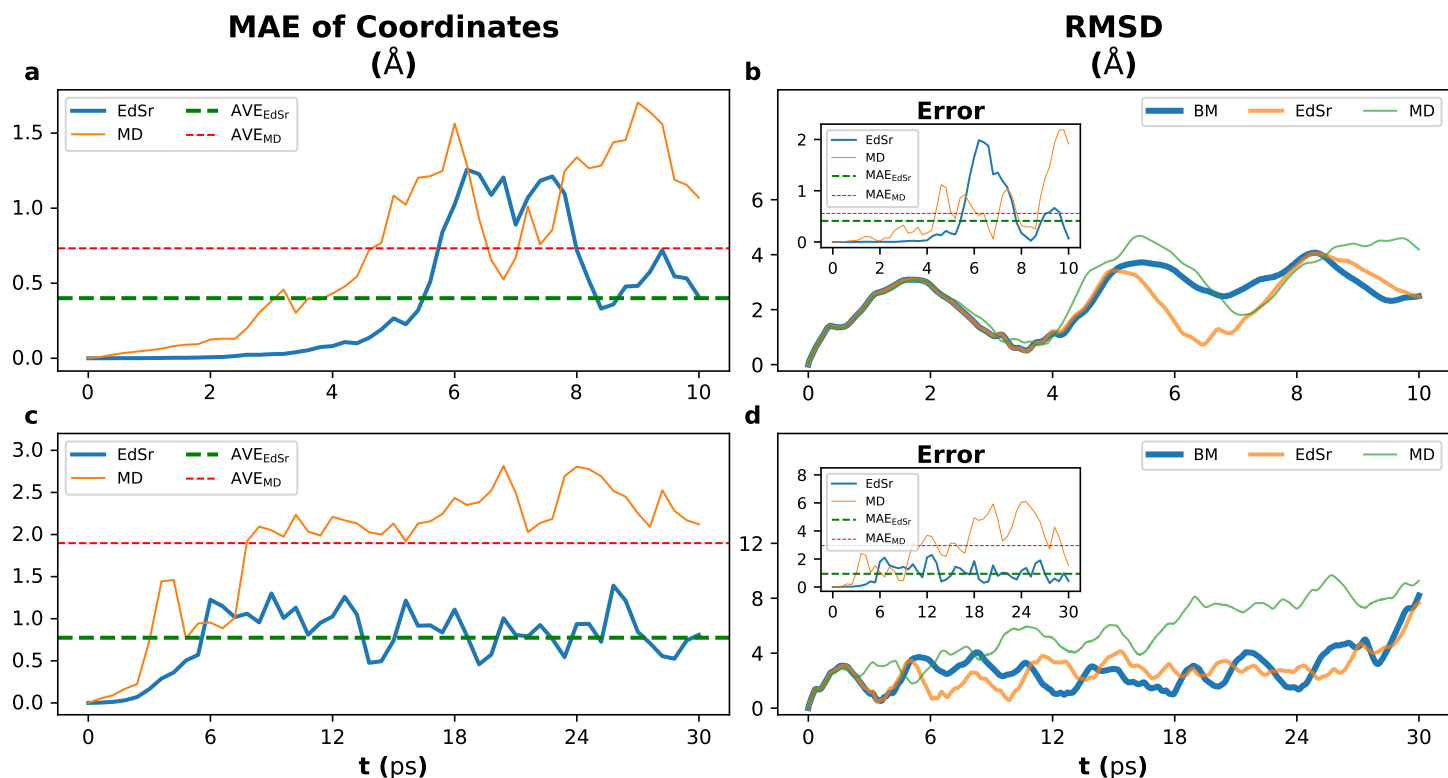


Fig. 6: MAEs between EdSr and BM groups, as well as between MD and BM groups of the atom coordinates of an indole molecule over time at $\Delta t = 1.0$ fs (a) and 3.0 fs (c), the two dashed lines in the two sub-figures represent the average MAEs. Time evolutions of RMSDs of BM, EdSr and MD group over time at $\Delta t = 1.0$ fs (b) and 3.0 fs (d), the insets are the AbsVEs between EdSr and BM, as well as between MD and BM groups, with their MAEs shown as the dashed lines.

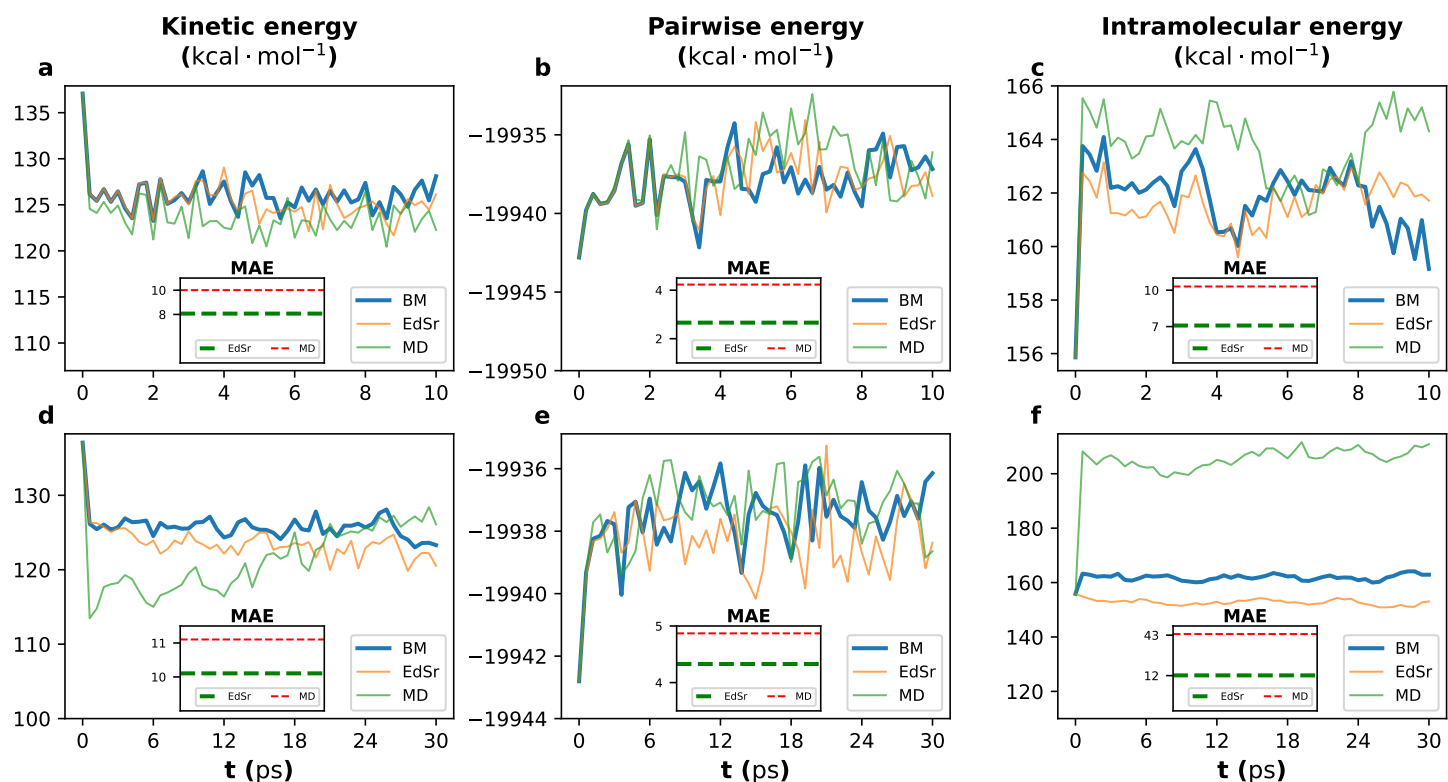


Fig. 7: Time evolutions of different energies obtained by BM, EdSr and MD groups in the all-atom MD simulations. (a-c) show the results of $\Delta t = 1.0$ fs, (d-f) show the results of $\Delta t = 3.0$ fs.

energy obtained via EdSr keeps at a much lower level than MD group during the whole simulation (Fig. 7f). We calculate the radial distribution functions (RDF) between indoles and zeolites, in which both EdSr and MD results match the BM group (Fig. S9a and c), indicating that the indole molecules in different simulations have similar relative positions. However, we find that the deviations of EdSr from BM increase as time evolves (Fig. 6 and 7), which results in the small deviation of velocity distribution of indoles on both EdSr and MD group after finishing the whole simulations (Fig. S9b and d). The comparisons of EdSr and MD groups versus BM at $\Delta t = 2.0$ fs, as well as the results of EdSr and BM group at $\Delta t = 4.0$ fs are provided from Fig. S10 to Fig. S12, which show that the structural properties obtained via EdSr are consistent with BM group at $\Delta t = 4.0$ fs, but the deviation of energies appears.

Coarse-Grained MD Simulation

In order to explore whether EdSr works well in more complicated systems with larger time and length scales, we set up the protein aqueous solution system to test the performance of EdSr [34]. We adopt the Martini coarse-grained (CG) force field 2.2 to convert the atomistic protein structure to Martini CG structure [43]. Each simulation box contains a single ubiquitin CG molecule with 163 CG beads, solvated in water CG beads which include 2224 P_4 beads and 247 BP_4 beads to prevent the solvent from freezing[44]. Then, we do a short energy minimization and equilibration of the CG system for 6 ns. After that we use the equilibrated CG configuration as the initial structure of the following three groups: VV integrator and small timestep $\Delta t = 1.0$ fs as benchmark (**BM group**), VV integrator for large timestep $\Delta t = 10.0$ fs, 20.0 fs as control groups (**MD group**), EdSr for large timestep $\Delta t = 10.0$ fs, 20.0 fs, 30.0 fs (**EdSr group**) to run simulations. The MD and EdSr simulations are also run under NVE ensemble with 1×10^4 steps, and the BM group performs for the same simulation time as the other two groups.

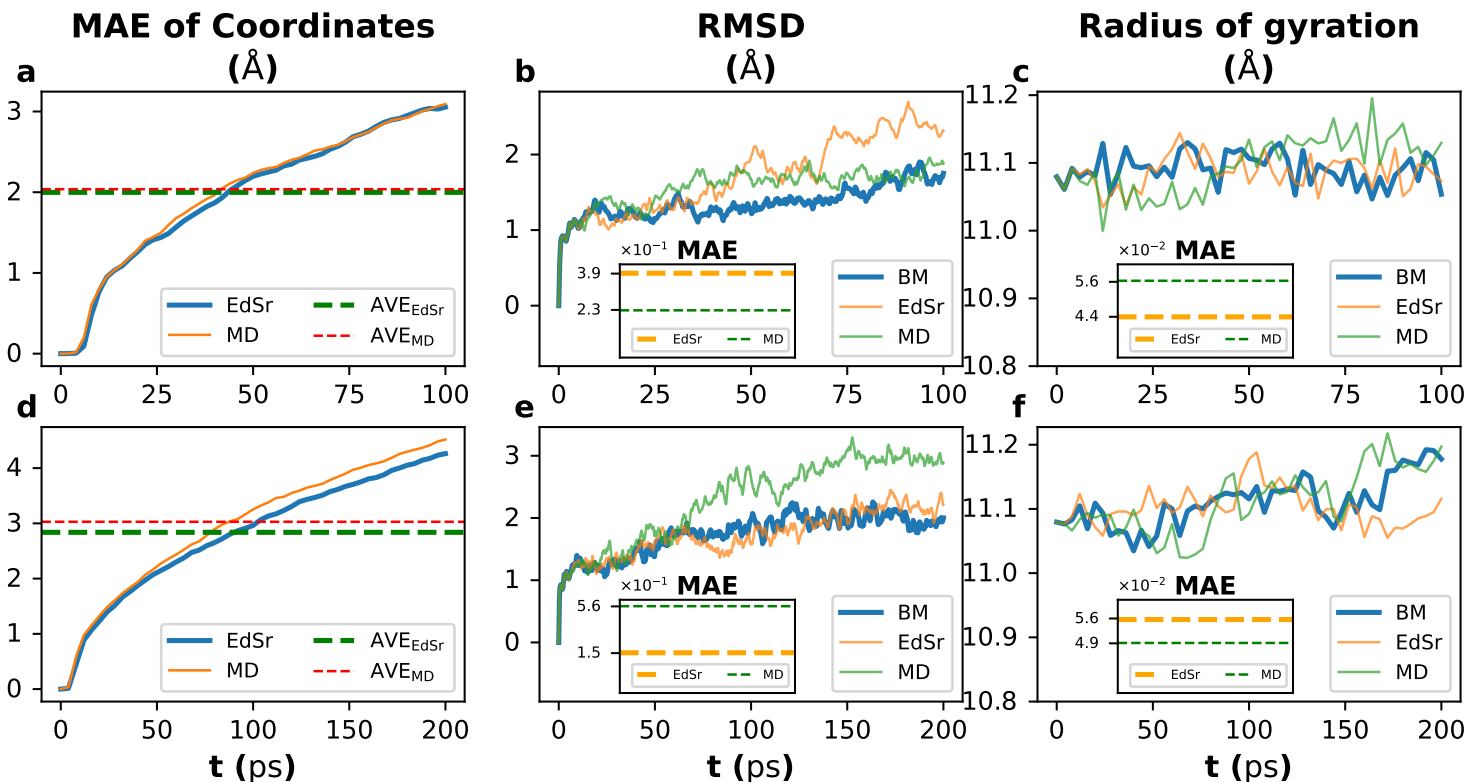


Fig. 8: MAEs between EdSr and BM groups, as well as between MD and BM groups of the particle coordinates of ubiquitin aqueous solution over time at $\Delta t = 10.0$ fs (a) and 20.0 fs (d), the two dashed lines in the two sub-figures represent the average MAEs. Time evolutions of RMSDs of BM, EdSr and MD group at $\Delta t = 10.0$ fs (b) and 20.0 fs (e), the insets are the MAEs of RMSDs from EdSr and MD groups by comparing with BM group. (c) and (f) shows radii of gyration of ubiquitin molecules in the three groups over time and their MAEs at $\Delta t = 10.0$ fs and 20.0 fs, respectively.

Similar as all-atom simulations, we also compute the MAEs of coordinates of all CG beads between MD and BM groups, as well as EdSr and BM groups (Fig. 8a and d), and find that both the MAEs from EdSr and MD increase as time evolves at $\Delta t = 10.0$ and 20.0 fs, the MAE from EdSr is a little smaller than MD at $\Delta t = 20.0$ fs (Fig. 8d). We also calculate the RMSDs from the three groups at $\Delta t = 10.0$ and 20.0 fs, which are shown in Fig. 8b and e, respectively. The MAE of RMSD from EdSr versus BM is slightly larger than that from MD group at $\Delta t = 10.0$ fs (inset of Fig. 8b), but much smaller than MD at $\Delta t = 20.0$ fs (inset of Fig. 8e). In addition, we investigate the configuration of ubiquitin by calculating the radius of gyration in the three groups at $\Delta t = 10.0$ and 20.0 fs, the results are exhibited in Fig. 8c and f, respectively. Both the results from EdSr and MD groups are

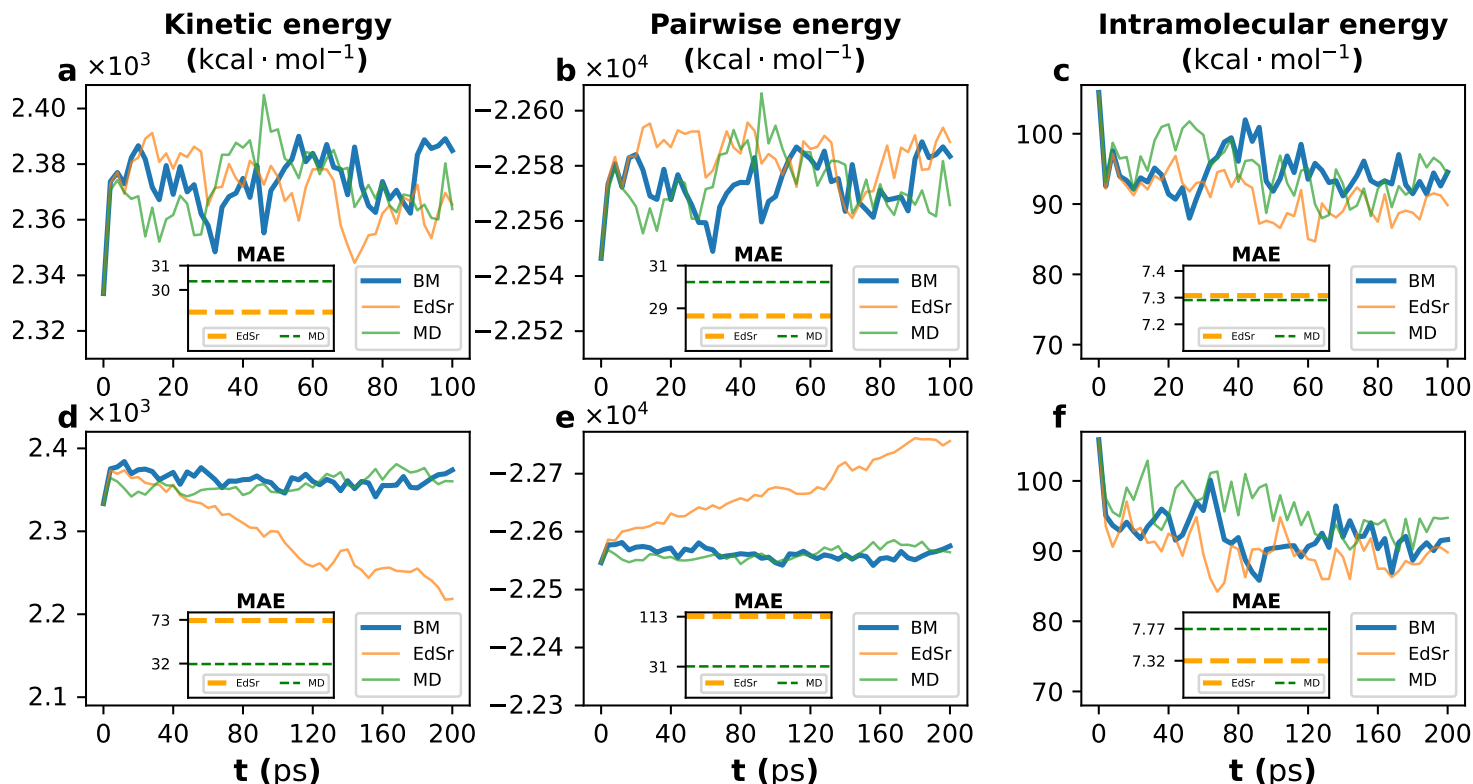


Fig. 9: Kinetic energy (a,d), pairwise energy (b,e), intramolecular energy (c,f) of BM, EdSr and MD groups over time. (a-c) shows the results of $\Delta t = 10.0$ fs and (d-f) shows the results of $\Delta t = 20.0$ fs. The insets exhibit the MAEs of EdSr and MD by comparing with BM group.

close to the BM group at the two selected timesteps, which indicates that the EdSr method can reproduce the conformation of macromolecule very well.

Then, we also compare thermodynamics features (kinetic energy, pairwise energy, intramolecular energy) in the three groups at $\Delta t = 10.0$ and 20.0 fs, the results are shown in Fig. 9. The kinetic, pairwise and intramolecular energies obtained via EdSr are similar as those from BM and MD groups at $\Delta t = 10.0$ fs (Fig. 9a-c). But the kinetic and pairwise energies from EdSr appear to be non-conservative at $\Delta t = 20.0$ fs (Fig. 9d and e), which results in the larger MAE from EdSr by comparing with BM group (insets of Fig. 9d and e). However, the MAE of intramolecular energy obtained in EdSr group is still lower than that from MD group, which demonstrates that protein still keeps stable in the EdSr group at large timestep (Fig. 9f). We compare the radial distribution functions between ubiquitin and water beads in the three groups. Although the deviation of kinetic and pairwise energies appears in EdSr at $\Delta t = 20.0$ fs, the distributions of water beads around the ubiquitin among the three groups are very similar (Fig. S13a and c). as well as the velocity distributions of the CG beads (Fig. S13b and d). We also perform the EdSr group at $\Delta t = 30.0$ fs and compare with the BM group (the MD group can not run at such a large timestep), the results of structural properties, thermodynamical features, radial distribution function and velocity distribution are available in Fig. S14, which also indicate that the EdSr group generate consistent results of RMSD, radius of gyration, radial distribution function with BM group. In order to understand the extent how water beads have an impact on EdSr in this system, we design another comparison groups without water beads and test the performance of EdSr at $\Delta t = 20.0$ and 30.0 fs, which are shown from Fig. S15 to S17. The differences of kinetic energies and potential energies between EdSr and BM groups are much smaller than the systems with water CG beads. Thus, we estimate that the deviation of EdSr may be related to the degree of freedom for a specific system. And it suggests that more degree of freedom in a system might lead to larger deviation of EdSr.

Conclusions and discussions

This paper proposes EdSr, a computational method based on Taylor expansion and Langevin dynamics, to expand up the time scale of MD simulation flexibly and dynamically. Rather than machine learning based method needed to be trained, EdSr endeavors to correctly generate next state from a specific state without cost of extra training and thousands of data. We not only design several experiments, including simple functions, ideal physical models and MD simulations, to verify the feasibility of EdSr, but also test the performance of EdSr by comparing with VV integrator. By combing with all the results, we demonstrate that EdSr shows incredible ability to perform at larger integration timestep in some systems (e.g. ideal spring, all-atom model

of *indole@Beta zeolite*), and does not work well in some cases (like $f(x) = x^3$ function, coarse-grained model of protein aqueous solution), which is up to the specific problem.

We build up the EdSr method based on the following reasons: firstly, we introduce a novel perspective to build a relationship between Taylor expansion and Langevin dynamics, which is introduced in **Methods**. In this paper, we transform the Taylor expansion into a kind of recursive process, in which each step resembles Langevin dynamics. So it is possible to use the recursive process to approximate Taylor Expansion with infinite term, which can eliminate the requirement for setting multiple parameter sets manually when selecting different partial differential equations or models. Secondly, we provide a special perspective to build a bridge between Taylor expansion and Markov process. Mathematically, we show the transformation from EdSr to 2-order Markov chain in **Methods**, which probably makes us understand the working mode of EdSr using probability density function. More importantly, EdSr make it possible to scale up the Δx in Taylor series, enabling tasks to be handled through parallel computing. For example, if EdSr can be applied at $\Delta t = 10$ for a given system, we can firstly use it to generate states at $t = 0, 1, \dots, 9$ in parallel, and then utilize these states to compute the states at $t = 10, 11, \dots, 19$ in parallel.

However, there is still more room for the EdSr approach to improve. First of all, it seems that EdSr does not work very well in some systems, because some functions or models might exceed the hypotheses mentioned in **Methods**. Therefore, EdSr should be test before embedding it into a specific system. Then, the maximum timestep of EdSr depends on the system it is adopted. In addition, executing a single step of EdSr is still time consuming. In future work, we will focus on the above problems and strive to reduce the computational cost of EdSr. Recently, it suggests that numerical difference method has been applied to enhance convolutional neural networks [45], which make it possible for convolutional neural networks with EdSr. Besides, we will also try to put the EdSr into applications, such as machine learning based on Diffusion Model, chemical reaction dynamics, etc. Although EdSr still has some limitations, we believe that it will be a promising approach in the future.

Methods

Preliminary

Before delving into the details of our method, we start by looking back some related theorems.

Path Integration A time-dependent variable can be described by the differential equation $X'(t) = \frac{dX}{dt} = f(X_t, t)$ for a general time t . Given an interval Δt , $X_{t+\Delta t}$ can be described as the following equation:

$$X_{t+\Delta t} = X_t + \int_t^{t+\Delta t} f(X_{t'}, t') dt' \quad (6)$$

Taylor Expansion In mathematics, given a real or complex-valued function $f(x)$, that is infinitely differentiable at a real or complex number x_0 , the Taylor expansion at $x_0 + \Delta x$ can be described as the following equation:

$$f(x_0 + \Delta x) = f(x_0) + \frac{f'(x_0)}{1!} \Delta x + \frac{f''(x_0)}{2!} (\Delta x)^2 + \dots + \frac{f^{(n)}(x_0)}{n!} (\Delta x)^n \quad (7)$$

where $n \rightarrow \infty$ and Δx is within domain of convergence, namely that $|\Delta x|$ is smaller than the radius of convergence r .

Fokker-Planck Equation For an Itô process driven by Brownian motion, the equation of motion can be described as:

$$dX_t = \mu(X_t, t)dt + \mathcal{D}(X_t, t)dW_t \quad (8)$$

where the $\mu(\cdot)$, $\mathcal{D}(\cdot)$ and W_t are drift, diffusion coefficient and Wiener process, respectively. In consequence, the corresponding Fokker-Planck equation for the probability density function (PDF) over time $p(X_t, t)$ is described as

$$\frac{d}{dt}p(X_t, t) = -\nabla_X [\mu(X_t, t)p(X_t, t)] + \nabla_X^2 [\mathcal{D}(X_t, t)p(X_t, t)] \quad (9)$$

However, in a practical application such as MD simulation, solving Fokker-Planck equation would be transformed to solving Langevin equation

$$MX'' = -\nabla U(X) - \gamma MX' + \sqrt{2M\gamma k_B T} \mathcal{B}(t) \quad (10)$$

where $\nabla U(X)$ is the gradient of interaction potential over X , γ , k_B , T are the damping constant, Boltzmann constant, temperature, respectively, and $\mathcal{B}(t)$ is a standard Gaussian process.

Exploratory dynamics Sampling with recursion (EdSr)

EdSr are based on the following hypotheses:

1. $X(t)$ and $X(t + \Delta t)$ are reasonable and accessible, which correspond to an actual state in a physical system. $X(t)$ is a continuous function in solving interval.
2. The function of the evolution over time $X(t)$ is infinitely differentiable at time t for an arbitrary physics system, namely that $\lim_{n \rightarrow +\infty} X^{(n)}(t) \neq \infty$.
3. Differential operator D acting on the $X(t)$ satisfies the following operations:

$$\begin{aligned} D_t(x(t) + y(t)) &= D_t x(t) + D_t y(t), & D_t(D_t x(t)) &= D_t^2 x(t) \\ D_t(ax(t)) &= aD_t x(t) = D_t x(t) \cdot a, & \text{where } a &= \text{const} \end{aligned}$$

4. $X^{(n-1)}(t)$ and $X^{(n)}(t)$ satisfy the following inequality:

$$\lim_{n \rightarrow +\infty} \frac{X^{(n)}(t)}{nX^{(n-1)}(t)} \neq 0$$

As we all know, if an initial state $X(t)$ was given, we can use the Newton's second law of motion ($F = ma$) to compute the force and get the next state $X_{t+\Delta t}$ by using the equation of motion ($X_{t+\Delta t} = X_t + v_t \Delta t + \frac{1}{2} \frac{F}{m} \Delta t^2$). However, it is obvious that Δt should be small enough if bias is expected to fall into a reasonable domain. Nevertheless, for a specific physical system, if the function $f(X_t, t)$ in Equation (6) could be determined, the state $X_{t+\Delta t}$ after a time interval Δt can be solved directly using Equation (6), thus greatly alleviating the constraint that Δt should be sufficiently small. Therefore, we are going to consider to solve the path integration.

However, it is difficult to get the $X'(t) = f(X_t, t)$ over time t in general. So we use partial integration to transform Equation (6), which is described as:

$$X(b) = X(a) + X'(a)\Delta t + \int_0^{\Delta t} yX''(b-y)dy \quad (11)$$

where b and a are equivalent to $t + \Delta t$ and t , respectively. According to First Mean Value Theorems for Definite Integrals, the Equation (11) is transformed to the following form:

$$X(b) = X(a) + X'(a)\Delta t + \frac{1}{2}X''(c)(\Delta t)^2 \quad c \in (a, b) \quad (12)$$

Equation (12) indicates that given a specific interval Δt , $X_{t+\Delta t}$ can be obtained from the X_t (generalized coordinates), the corresponding first order derivative $X'(t)$ (generalized velocities) and the second order derivative of a point c between t and $t + \Delta t$. Consequently, the aim to solve the $f(X_t, t)$ transforms to the aim to solve the point c .

According to the hypothesis (2), Equation (6) can be expanded by multi-time partial integration and we replace the derivative by the differential operator D . Therefore the equation can be rewritten to the form:

$$\begin{aligned} X(b) &= X(a) + \underbrace{DX(a)\Delta t + \frac{1}{2!}D^2X(a)(\Delta t)^2 + \dots + \frac{1}{n!}D^nX(a)(\Delta t)^n}_{\text{the first term}} \\ &+ \underbrace{\frac{1}{(n+1)!} \int_0^{\Delta t} X^{(n+1)}(b-y)dy^{n+1}}_{\text{the second term}} \end{aligned} \quad (13)$$

For the last three terms in “the first term” in Equation (13), according to hypothesis (3), we can get a new form:

$$\begin{aligned}
& \frac{1}{(n-2)!} D^{n-2} X(a) (\Delta t)^{n-2} + \frac{1}{(n-1)!} D^n X(a) (\Delta t)^{n-1} + \frac{1}{n!} D^n X(a) (\Delta t)^n \\
&= \frac{1}{(n-2)!} D^{n-2} \left(X(a) + \frac{1}{n-1} DX(a) \Delta t + \frac{1}{(n-1)n} D^2 X(a) (\Delta t)^2 \right) (\Delta t)^{n-2} \\
&= \frac{1}{(n-2)!} D^{n-2} \left(X(a) + \frac{1}{n-1} \left(DX(a) \Delta t + \frac{1}{n} D^2 X(a) (\Delta t)^2 \right) \right) (\Delta t)^{n-2}
\end{aligned} \tag{14}$$

where $DX(a) = \frac{dX}{dt}$, $D^2 X(a) = \frac{d^2 X}{dt^2}$ are the first-order and the second-order derivatives over time t , respectively. For “the second term” in Equation (13), because $X(b)$ exists according to hypothesis (1), the series is convergent. Thereby, “the second term” tends to be 0 as $n \rightarrow \infty$. So we assume “the second term” to 0. Inspired by the Langevin dynamics in Equation (10), $D^2 X(a)$ are replaced by $-\frac{\nabla_X U(X(a))}{M}$ and we approximate the point c in Equation (12) with a recursion like Langevin dynamics, where M denotes mass.

Finally, the part of displacement of EdSr can be rewritten as the following form:

$$X_{n-1} = X_N + \frac{1}{2n-1} \left(X'_N \Delta t - \frac{1}{2n} \frac{\nabla_X U(X_n)}{M} (\Delta t)^2 \right), \quad n \text{ for } N \text{ to } 1 \tag{15}$$

where X_0, X_N, X'_N denote $X(b), X(a), X'(a)$ respectively. According to the definition of derivative, the part of velocity of EdSr can be expressed as:

$$\begin{cases} X_{n-1} = X_N + \frac{1}{2n-2} \left(X'_N \Delta t - \frac{1}{2n-1} \frac{\nabla_X U(X_n)}{M} (\Delta t)^2 \right), & n \text{ for } N \text{ to } 2 \\ X'_0 = X'_N - \frac{\nabla_X U(X_1)}{M} \Delta t, & n = 1 \end{cases} \tag{16}$$

where X'_0 denotes $X'(b)$. The framework of the EdSr is summarized in Algorithm 1.

Bridge between EdSr and Markov process

In this section, we make a bridge between EdSr and Markov process. Mathematically, we can transform EdSr to 2-order Markov chain. Here we derive the transformation process briefly. In general, the initial velocities of particles in a system is sampled from Maxwell-Boltzmann distribution, which means $v \sim \mathcal{N}(0, \frac{k_B T}{M})$. The logarithmic of probability density function $\log p(x)$ can be described as the potential energy $U(x)$ divided by $k_B T$, namely that $\log p(x) = -\frac{U(x)}{k_B T}$. We set $\frac{k_B T}{M} = \sigma^2$, Equation (15) can be rewritten as the following form:

$$\begin{aligned}
X_{n-1} &= X_N + \left[\frac{1}{2n-1} - \frac{1}{2n} \right] \sigma^2 \nabla_X \log p(X_n) (\Delta t)^2 + \frac{1}{2n-1} \sigma (\Delta t) \epsilon, \quad \text{where } \epsilon \sim \mathcal{N}(0, I) \\
X_{n-2} &= X_N + \left[\frac{1}{2n-3} - \frac{1}{2n-2} \right] \sigma^2 \nabla_X \log p(X_{n-1}) (\Delta t)^2 + \frac{1}{2n-3} \sigma (\Delta t) \epsilon, \quad \text{where } \epsilon \sim \mathcal{N}(0, I)
\end{aligned}$$

We can get the 2-order Markov process similar to Equation (8) by using $X_{n-2} - X_{n-1}$.

$$\begin{aligned}
X_{n-2} - X_{n-1} &= \sigma^2 (\Delta t)^2 \left\{ \left[\frac{1}{2n-3} - \frac{1}{2n-2} \right] \nabla_X \log p(x_{n-1}) - \left[\frac{1}{2n-1} - \frac{1}{2n} \right] \nabla_X \log p(x_n) \right\} \\
&\quad + \sigma (\Delta t) \left(\frac{1}{2n-3} - \frac{1}{2n-1} \right) \epsilon, \quad \text{where } \epsilon \sim \mathcal{N}(0, I)
\end{aligned}$$

Code and data availability

All codes about this paper is publicly available at <https://github.com/haiming-Cao/EdSr>

Algorithm 1 Exploratorily dynamics Sampling with recursion

Input: Initial state $x_t = X(t)$, $v_t = X'(t)$, timestep Δt , mass M , force field solver $\epsilon(\cdot)$.

Max Iteration N ;

```
1: Initialize:  $x_t$  deepcopy to  $x_n$  and  $v_n$ 
2: // Displacement Iteration;
3: for  $n = N$  to 1 do
4:    $dx = v_t \Delta t + \frac{1}{2n} M^{-1} \epsilon(x_n) (\Delta t)^2$ 
5:    $x_n = x_t + \frac{1}{2n-1} dx$ 
6: end for
7: // Velocity Iteration;
8: for  $n = N$  to 1 do
9:    $dv = \frac{1}{2n-1} M^{-1} \epsilon(v_n) \Delta t$ 
10:  if  $n > 1$  then
11:     $v_n = x_t + \frac{1}{2n-2} (v_t + dv) \Delta t$ 
12:  else
13:     $v_{t+\Delta t} = v_t + dv$ 
14:  end if
15: end for
16:  $x_{t+\Delta t} = x_n$ 
17: return  $x_{t+\Delta t}$ ,  $v_{t+\Delta t}$ 
```

Acknowledgement

We appreciate the financial support from the Guangdong Basic and Applied Basic Research Foundation (2023A1515012535, 2022A1515010873) and National Natural Science Foundation of China (no. 22003080).

References

- [1] B. J. Alder and T. E. Wainwright. Phase Transition for a Hard Sphere System. *J. Chem. Phys.*, 27(5):1208–1209, November 1957. ISSN 0021-9606. doi: 10.1063/1.1743957. URL <https://aip.scitation.org/doi/abs/10.1063/1.1743957>.
- [2] Florian Müller-Plathe. Coarse-Graining in Polymer Simulation: From the Atomistic to the Mesoscopic Scale and Back. *ChemPhysChem*, 3(9):754–769, 2002. ISSN 1439-7641. doi: 10.1002/1439-7641(20020916)3:9<754::AID-CPHC754>3.0.CO;2-U. URL [http://onlinelibrary.wiley.com/doi/10.1002/1439-7641\(20020916\)3:9<754::AID-CPHC754>3.0.CO;2-U/abstract](http://onlinelibrary.wiley.com/doi/10.1002/1439-7641(20020916)3:9<754::AID-CPHC754>3.0.CO;2-U/abstract).
- [3] Christine Peter and Kurt Kremer. Multiscale simulation of soft matter systems – from the atomistic to the coarse-grained level and back. *Soft Matter*, 5(22):4357–4366, November 2009. ISSN 1744-6848. doi: 10.1039/B912027K. URL <http://pubs.rsc.org/en/content/articlelanding/2009/sm/b912027k>.
- [4] M. P. Allen and D. J. Tildesley. *Computer Simulation of Liquids*. Clarendon Press, Oxford, 1987.
- [5] Tingting Li, Chengen Ho, Mengxi Han, Pai Peng, Junjie Chen, Yong Huang, Bin Li, and Qiang Chen. Zeolite encapsulation of indole as an antibacterial with controllable release property. *Langmuir*, 39(29):10122–10132, 2023. doi: 10.1021/acs.langmuir.3c01063. URL <https://doi.org/10.1021/acs.langmuir.3c01063>. PMID: 37429834.
- [6] Josep Rizo, Levent Sari, Klaudia Jaczynska, Christian Rosenmund, and Milo M. Lin. Molecular mechanism underlying snare-mediated membrane fusion enlightened by all-atom molecular dynamics simulations. *Proc. Natl. Acad. Sci.*, 121(16):e2321447121, 2024. doi: 10.1073/pnas.2321447121. URL <https://www.pnas.org/doi/abs/10.1073/pnas.2321447121>.
- [7] Sebastian Kmiecik, Dominik Gront, Michal Kolinski, Lukasz Wieteska, Aleksandra Elzbieta Dawid, and Andrzej Kolinski. Coarse-Grained Protein Models and Their Applications. *Chem. Rev.*, 116(14):7898–7936, July 2016. ISSN 0009-2665. doi: 10.1021/acs.chemrev.6b00163. URL <https://doi.org/10.1021/acs.chemrev.6b00163>.
- [8] Siewert J. Marrink, H. Jelger Risselada, Serge Yefimov, D. Peter Tieleman, and Alex H. de Vries. The MARTINI Force Field: Coarse Grained Model for Biomolecular Simulations. *J. Phys. Chem. B*, 111(27):7812–7824, 2007. ISSN 1520-6106. doi: 10.1021/jp071097f. URL <http://dx.doi.org/10.1021/jp071097f>.
- [9] Emiliano Brini, Elena A. Algaer, Pritam Ganguly, Chunli Li, Francisco Rodríguez-Roperó, and Nico F. A. van der Vegt. Systematic coarse-graining methods for soft matter simulations – a review. *Soft Matter*, 9(7):2108–2119, February 2013. ISSN 1744-6848. doi: 10.1039/C2SM27201F. URL <http://pubs.rsc.org/en/content/articlelanding/2013/sm/c2sm27201f>.

- [10] Ksenia Korshunova, Julius Kiuru, Juho Liekkinen, Giray Enkavi, Ilpo Vattulainen, and Bart M. H. Bruininks. Martini 3 oligomers: A scalable approach for multimers and fibrils in gromacs. *J. Chem. Theory Comput.*, 20(17):7635–7645, 2024. doi: 10.1021/acs.jctc.4c00677. URL <https://doi.org/10.1021/acs.jctc.4c00677>. PMID: 39189419.
- [11] Petteri Vainikka and Siewert J. Marrink. Martini 3 coarse-grained model for second-generation unidirectional molecular motors and switches. *J. Chem. Theory Comput.*, 19(2):596–604, 2023. doi: 10.1021/acs.jctc.2c00796. URL <https://doi.org/10.1021/acs.jctc.2c00796>. PMID: 36625495.
- [12] Luís Borges-Araújo, Ana C. Borges-Araújo, Tugba Nur Ozturk, Daniel P. Ramirez-Echemendia, Balázs Fábíán, Timothy S. Carpenter, Sebastian Thallmair, Jonathan Barnoud, Helgi I. Ingólfsson, Gerhard Hummer, D. Peter Tieleman, Siewert J. Marrink, Paulo C. T. Souza, and Manuel N. Melo. Martini 3 coarse-grained force field for cholesterol. *J. Chem. Theory Comput.*, 19(20):7387–7404, 2023. doi: 10.1021/acs.jctc.3c00547. URL <https://doi.org/10.1021/acs.jctc.3c00547>. PMID: 37796943.
- [13] Yusong Wang, Tong Wang, Shaoning Li, Xinheng He, Mingyu Li, Zun Wang, Nanning Zheng, Bin Shao, and Tie-Yan Liu. Enhancing geometric representations for molecules with equivariant vector-scalar interactive message passing. *Nat. Commun.*, 15(1):313, January 2024. ISSN 2041-1723. doi: 10.1038/s41467-023-43720-2. URL <https://www.nature.com/articles/s41467-023-43720-2>. Publisher: Nature Publishing Group.
- [14] Kristof Schütt, Oliver Unke, and Michael Gastegger. Equivariant message passing for the prediction of tensorial properties and molecular spectra. In *International Conference on Machine Learning*, pages 9377–9388. PMLR, 2021.
- [15] Sandro Wieser and Egbert Zojer. Machine learned force-fields for an ab-initio quality description of metal-organic frameworks. *NPJ Comput. Mater.*, 10(1):18, 2024.
- [16] Loup Verlet. Computer “experiments” on classical fluids. i. thermodynamical properties of lennard-jones molecules. *Phys. Rev.*, 159:98–103, Jul 1967. doi: 10.1103/PhysRev.159.98. URL <https://link.aps.org/doi/10.1103/PhysRev.159.98>.
- [17] CW Gear. Numerical initial value problems in ordinary differential equations, 1971.
- [18] M. Tuckerman, B. J. Berne, and G. J. Martyna. Reversible multiple time scale molecular dynamics. *J. Chem. Phys.*, 97(3):1990–2001, 08 1992. ISSN 0021-9606. doi: 10.1063/1.463137. URL <https://doi.org/10.1063/1.463137>.
- [19] Aidan P. Thompson, H. Metin Aktulga, Richard Berger, Dan S. Bolintineanu, W. Michael Brown, Paul S. Crozier, Pieter J. in ’t Veld, Axel Kohlmeyer, Stan G. Moore, Trung Dac Nguyen, Ray Shan, Mark J. Stevens, Julien Tranchida, Christian Trott, and Steven J. Plimpton. LAMMPS - a flexible simulation tool for particle-based materials modeling at the atomic, meso, and continuum scales. *Comput. Phys. Commun.*, 271:108171, 2022. ISSN 0010-4655. doi: <https://doi.org/10.1016/j.cpc.2021.108171>. URL <https://www.sciencedirect.com/science/article/pii/S0010465521002836>.
- [20] Sander Pronk, Szilárd Páll, Roland Schulz, Per Larsson, Pär Bjelkmar, Rossen Apostolov, Michael R. Shirts, Jeremy C. Smith, Peter M. Kasson, David van der Spoel, Berk Hess, and Erik Lindahl. GROMACS 4.5: a high-throughput and highly parallel open source molecular simulation toolkit. *Bioinformatics*, 29(7):845–854, 02 2013. ISSN 1367-4803. doi: 10.1093/bioinformatics/btt055. URL <https://doi.org/10.1093/bioinformatics/btt055>.
- [21] David Van Der Spoel, Erik Lindahl, Berk Hess, Gerrit Groenhof, Alan E. Mark, and Herman J. C. Berendsen. Gromacs: Fast, flexible, and free. *J. Comput. Chem.*, 26(16):1701–1718, 2005. doi: <https://doi.org/10.1002/jcc.20291>. URL <https://onlinelibrary.wiley.com/doi/abs/10.1002/jcc.20291>.
- [22] Miles Cranmer, Sam Greidanus, Stephan Hoyer, Peter Battaglia, David Spergel, and Shirley Ho. Lagrangian neural networks. In *ICLR 2020 Workshop on Integration of Deep Neural Models and Differential Equations*, 2020.
- [23] Michael Lutter, Christian Ritter, and Jan Peters. Deep lagrangian networks: Using physics as model prior for deep learning. In *International Conference on Learning Representations*, 2018.
- [24] Samuel Greidanus, Misko Dzamba, and Jason Yosinski. Hamiltonian neural networks. *Advances in neural information processing systems*, 32, 2019.
- [25] Andrew Sosanya and Sam Greidanus. Dissipative hamiltonian neural networks: Learning dissipative and conservative dynamics separately. *arXiv preprint arXiv:2201.10085*, 2022.
- [26] Yang Song, Jascha Sohl-Dickstein, Diederik P. Kingma, Abhishek Kumar, Stefano Ermon, and Ben Poole. Score-based generative modeling through stochastic differential equations, 2020. URL <https://arxiv.org/abs/2011.13456>.
- [27] Jascha Sohl-Dickstein, Eric Weiss, Niru Maheswaranathan, and Surya Ganguli. Deep unsupervised learning using nonequilibrium thermodynamics. In Francis Bach and David Blei, editors, *Proceedings of the 32nd International Conference on Machine Learning*, volume 37 of *Proceedings of Machine Learning Research*, pages 2256–2265, Lille, France, 07–09 Jul 2015. PMLR. URL <https://proceedings.mlr.press/v37/sohl-dickstein15.html>.

- [28] Jonathan Ho, Ajay Jain, and Pieter Abbeel. Denoising diffusion probabilistic models. In *Advances in Neural Information Processing Systems*, volume 33, pages 6840–6851. Curran Associates, Inc., 2020. URL <https://proceedings.neurips.cc/paper/2020/hash/4c5bcfec8584af0d967f1ab10179ca4b-Abstract.html>.
- [29] Fang Wu and Stan Z Li. Diffmd: a geometric diffusion model for molecular dynamics simulations. In *Proceedings of the AAAI Conference on Artificial Intelligence*, volume 37, pages 5321–5329, 2023.
- [30] Mathias Schreiner, Ole Winther, and Simon Olsson. Implicit transfer operator learning: Multiple time-resolution models for molecular dynamics. *Advances in Neural Information Processing Systems*, 36, 2024.
- [31] Tim Hsu, Babak Sadigh, Vasily Bulatov, and Fei Zhou. Score dynamics: Scaling molecular dynamics with picoseconds time steps via conditional diffusion model. *J. Chem. Theory Comput.*, 20(6):2335–2348, 2024. ISSN 1549-9618, 1549-9626. doi: 10.1021/acs.jctc.3c01361. URL <https://pubs.acs.org/doi/10.1021/acs.jctc.3c01361>.
- [32] Andrew Morton and Brian W. Matthews. Specificity of ligand binding in a buried nonpolar cavity of t4 lysozyme: Linkage of dynamics and structural plasticity. *Biochemistry*, 34(27):8576–8588, 1995. ISSN 0006-2960, 1520-4995. doi: 10.1021/bi00027a007. URL <https://pubs.acs.org/doi/abs/10.1021/bi00027a007>.
- [33] Hwankyu Lee, Alex H. de Vries, Siewert-Jan Marrink, and Richard W. Pastor. A coarse-grained model for polyethylene oxide and polyethylene glycol: Conformation and hydrodynamics. *J. Phys. Chem. B*, 113(40):13186–13194, 2009. ISSN 1520-6106. doi: 10.1021/jp9058966. URL <https://doi.org/10.1021/jp9058966>. Publisher: American Chemical Society.
- [34] Senadhi Vijay-Kumar, Charles E. Bugg, and William J. Cook. Structure of ubiquitin refined at 1.8Å resolution. *J. Mol. Biol.*, 194(3):531–544, 1987. ISSN 0022-2836. doi: [https://doi.org/10.1016/0022-2836\(87\)90679-6](https://doi.org/10.1016/0022-2836(87)90679-6). URL <https://www.sciencedirect.com/science/article/pii/0022283687906796>.
- [35] J.R. Dormand and P.J. Prince. A family of embedded runge-kutta formulae. *J. Comput. Appl. Math.*, 6(1):19–26, 1980. ISSN 0377-0427. doi: [https://doi.org/10.1016/0771-050X\(80\)90013-3](https://doi.org/10.1016/0771-050X(80)90013-3). URL <https://www.sciencedirect.com/science/article/pii/0771050X80900133>.
- [36] Klaus-Peter Schröder, Joachim Sauer, Maurice Leslie, C. Richard, A. Catlow, and John M. Thomas. Bridging hydrodyl groups in zeolitic catalysts: a computer simulation of their structure, vibrational properties and acidity in protonated faujasites (h-y zeolites). *Chem. Phys. Lett.*, 188(3):320–325, 1992. ISSN 0009-2614. doi: [https://doi.org/10.1016/0009-2614\(92\)90030-Q](https://doi.org/10.1016/0009-2614(92)90030-Q). URL <https://www.sciencedirect.com/science/article/pii/000926149290030Q>.
- [37] M. J. Sanders, M. Leslie, and C. R. A. Catlow. Interatomic potentials for sio2. *J. Chem. Soc., Chem. Commun.*, pages 1271–1273, 1984. doi: 10.1039/C39840001271. URL <http://dx.doi.org/10.1039/C39840001271>.
- [38] Sudhir K. Sahoo and Nisanth N. Nair. Interfacing the core-shell or the drude polarizable force field with car-parrinello molecular dynamics for qm/mm simulations. *Front. Chem.*, 6, 2018. ISSN 2296-2646. doi: 10.3389/fchem.2018.00275. URL <https://www.frontiersin.org/journals/chemistry/articles/10.3389/fchem.2018.00275>.
- [39] Fateme S. Emami, Valeria Puddu, Rajiv J. Berry, Vikas Varshney, Siddharth V. Patwardhan, Carole C. Perry, and Hendrik Heinz. Force field and a surface model database for silica to simulate interfacial properties in atomic resolution. *Chem. Mater.*, 26(8):2647–2658, 2014. doi: 10.1021/cm500365c. URL <https://doi.org/10.1021/cm500365c>.
- [40] Peipei Li, Hao Chen, Jennifer A. Schott, Bo Li, Yaping Zheng, Shannon M. Mahurin, De-en Jiang, Guokai Cui, Xunxiang Hu, Yangyang Wang, Lengwan Li, and Sheng Dai. Porous liquid zeolites: hydrogen bonding-stabilized h-zsm-5 in branched ionic liquids. *Nanoscale*, 11:1515–1519, 2019. doi: 10.1039/C8NR07337F. URL <http://dx.doi.org/10.1039/C8NR07337F>.
- [41] Shūichi Nosé. A molecular dynamics method for simulations in the canonical ensemble. *Mol. Phys.*, 52(2):255–268, 1984. doi: 10.1080/00268978400101201. URL <https://doi.org/10.1080/00268978400101201>.
- [42] William G. Hoover. Canonical dynamics: Equilibrium phase-space distributions. *Phys. Rev. A*, 31:1695–1697, Mar 1985. doi: 10.1103/PhysRevA.31.1695. URL <https://link.aps.org/doi/10.1103/PhysRevA.31.1695>.
- [43] Djurre H. de Jong, Gurpreet Singh, W. F. Drew Bennett, Clement Arnarez, Tsjerk A. Wassenaar, Lars V. Schäfer, Xavier Periole, D. Peter Tieleman, and Siewert J. Marrink. Improved parameters for the martini coarse-grained protein force field. *J. Chem. Theory Comput.*, 9(1):687–697, 2013. doi: 10.1021/ct300646g. URL <https://doi.org/10.1021/ct300646g>. PMID: 26589065.
- [44] Siewert J. Marrink, H. Jelger Risselada, Serge Yefimov, D. Peter Tieleman, and Alex H. de Vries. The martini force field: Coarse grained model for biomolecular simulations. *J. Phys. Chem. B*, 111(27):7812–7824, 2007. doi: 10.1021/jp071097f. URL <https://doi.org/10.1021/jp071097f>. PMID: 17569554.
- [45] Qi Wang, Zijun Gao, Mingxiu Sui, Taiyuan Mei, Xiaohan Cheng, and Iris Li. Enhancing convolutional neural networks with higher-order numerical difference methods. In *2024 5th International Conference on Big Data & Artificial Intelligence & Software Engineering (ICBASE)*, pages 38–42, 2024. doi: 10.1109/ICBASE63199.2024.10762728.

Supplementary Information for EdSr: A Novel End-to-End Approach for State-Space Sampling in Molecular Dynamics Simulation

Hai-Ming Cao¹, Bin Li^{1*}

December 31, 2024

arXiv:2412.20978v1 [physics.comp-ph] 30 Dec 2024

Contents

Simple function	2
Ideal Spring	4
Ideal Pendulum	5
Two Body Model	6
Diffusion of Indole in Zeolite	7
Ubiquitin	10
Ubiquitin without Water Beads	12

¹School of Chemical Engineering and Technology, Sun Yat-Sen University, Zhuhai 519082, China. E-mail: libin76@mail.sysu.edu.cn

1 Simple function

Here we show the results from EdSr of $y = \frac{1}{1+e^{-x}}$ which is named sigmoid function, as well as $y = x^3$ and $y = x^2 - 2x - 5$. We use the source functions and their corresponding derivatives as ground truth (GT).

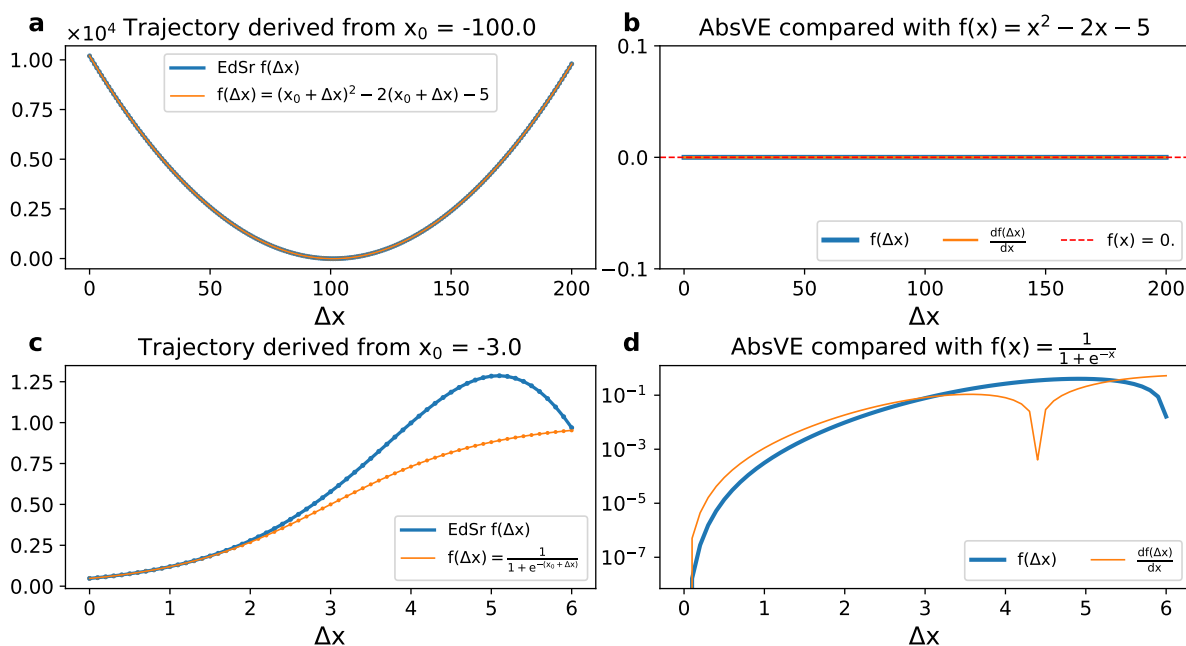


Fig. S1: Results of the first group of sub-experiments of $f(x) = x^2 - 2x - 5$ and sigmoid function. (a) GT of $f(x) = x^2 - 2x - 5$ and the result generated by EdSr, (b) absolute value of error (AbsVE) between function $f(x) = x^2 - 2x - 5$ and the corresponding derivative between GT and EdSr, (c) GT of $f(x) = \frac{1}{1+e^{-x}}$ and the result generated by EdSr, (d) AbsVE between function $f(x) = \frac{1}{1+e^{-x}}$ and the corresponding derivative between GT and EdSr.

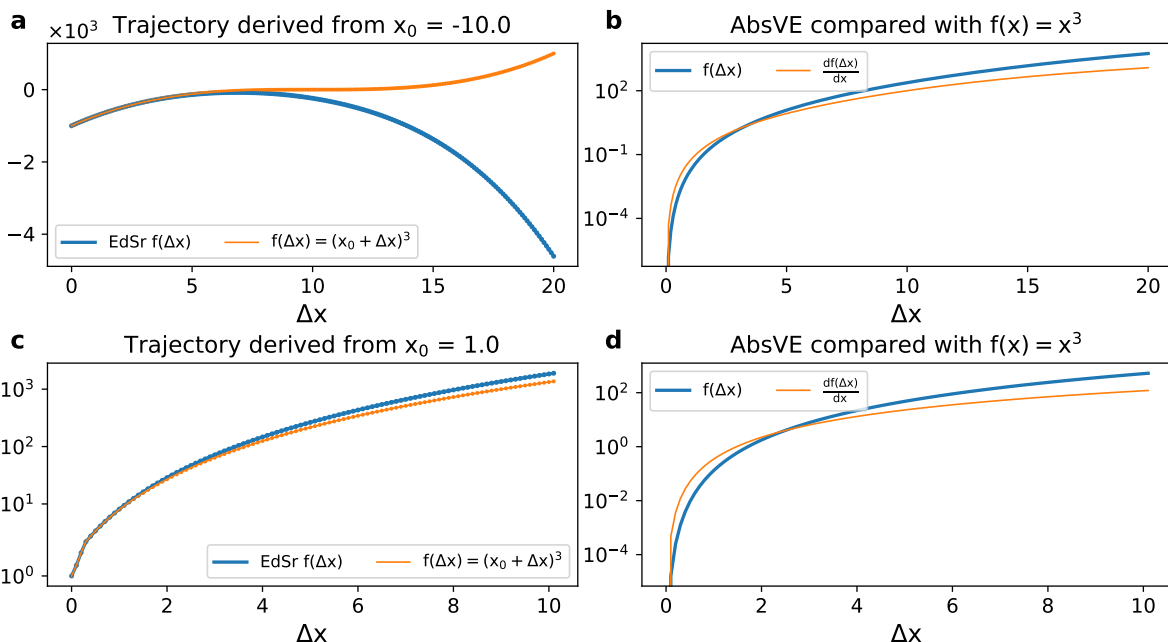


Fig. S2: Results of the first group of sub-experiments of $f(x) = x^3$ with different initial point x_0 . (a), (c) denotes GT and the results generated by EdSr derived from $x_0 = -10.0$ and 1.0 , respectively. (b), (d) denotes the corresponding AbsVEs between GT and EdSr of the function and their derivatives.

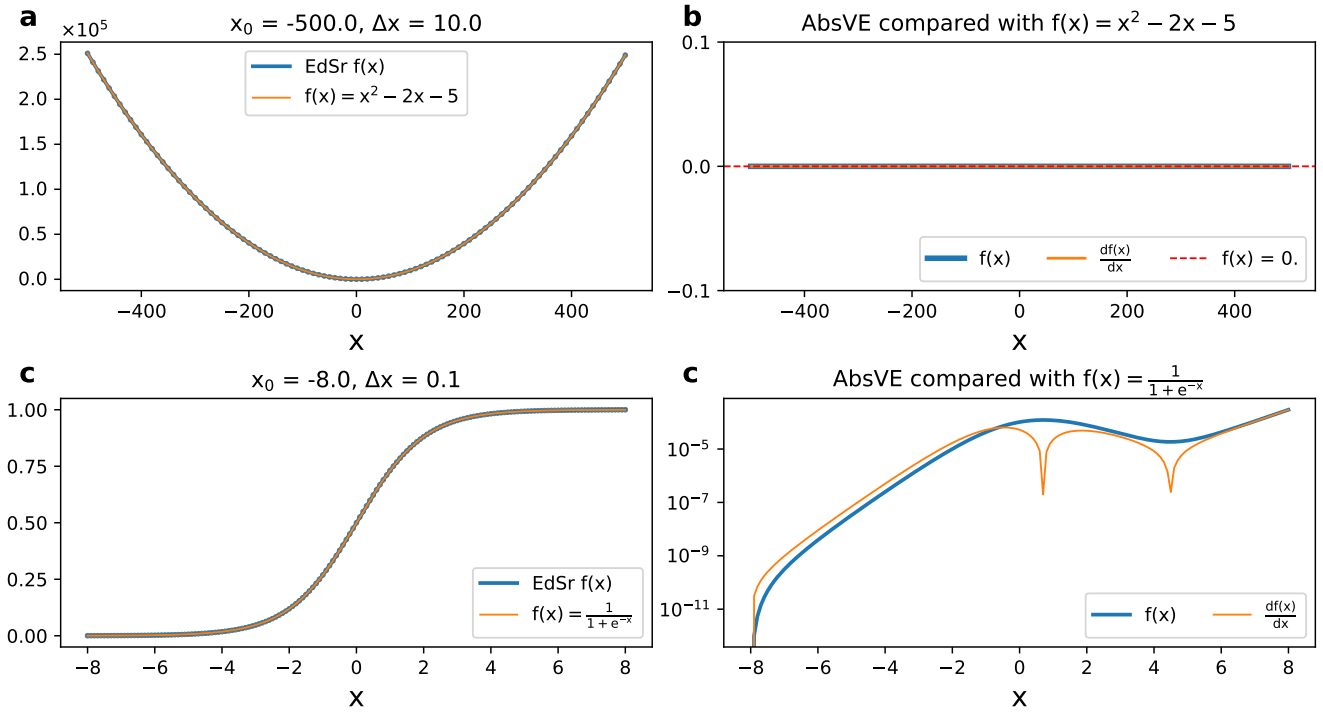


Fig. S3: Results of the second group of sub-experiments of $y = x^2 - 2x - 5$ and sigmoid function with different initial point x_0 and different Δx .

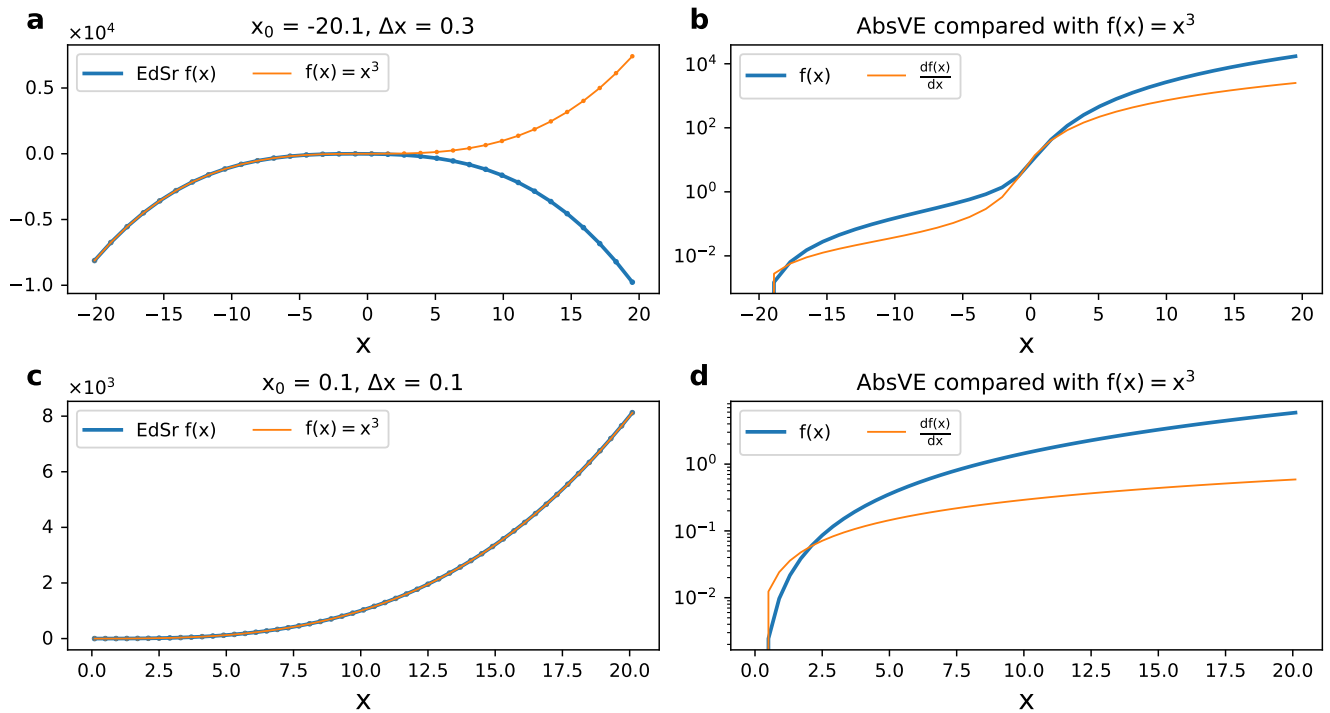


Fig. S4: Results of the second group of sub-experiments of $y = x^3$ with different initial point x_0 and different Δx .

2 Ideal Spring

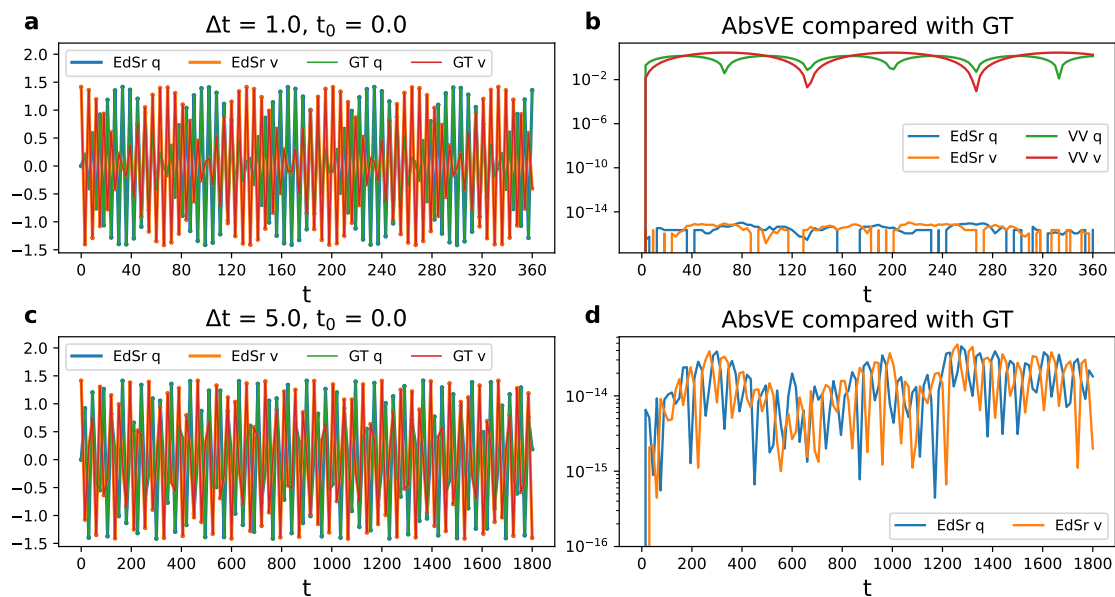


Fig. S5: Results of the second group of sub-experiments of ideal spring with different Δt values. (a), (b) show the comparisons of generalized coordinates q and velocities v between EdSr and GT, and the corresponding AbsVEs at $\Delta t = 1.0$. (c), (d) denote the results with $\Delta t = 5.0$. The AbsVEs between VV and GT are not shown at $\Delta t = 5.0$ as they are very huge.

3 Ideal Pendulum

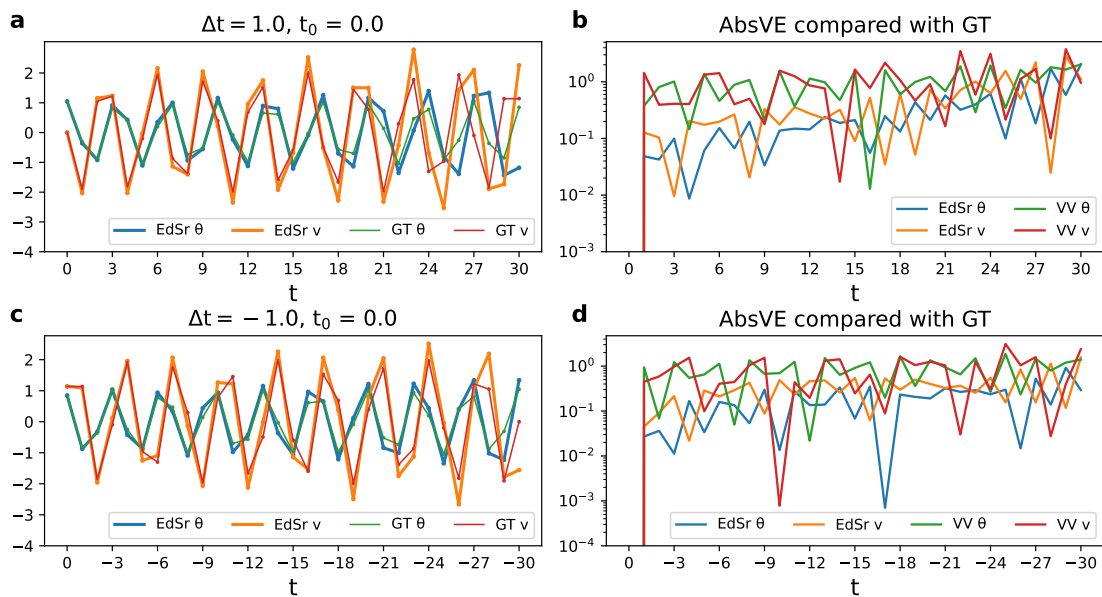


Fig. S6: Results of the second group of sub-experiments of ideal pendulum with different Δt values. (a), (b) show the comparisons of angles θ and angular velocities v between EdSr and GT, and the corresponding AbsVEs with $\Delta t = 1.0$. (c), (d) denote the results with $\Delta t = -1.0$.

4 Two Body Model

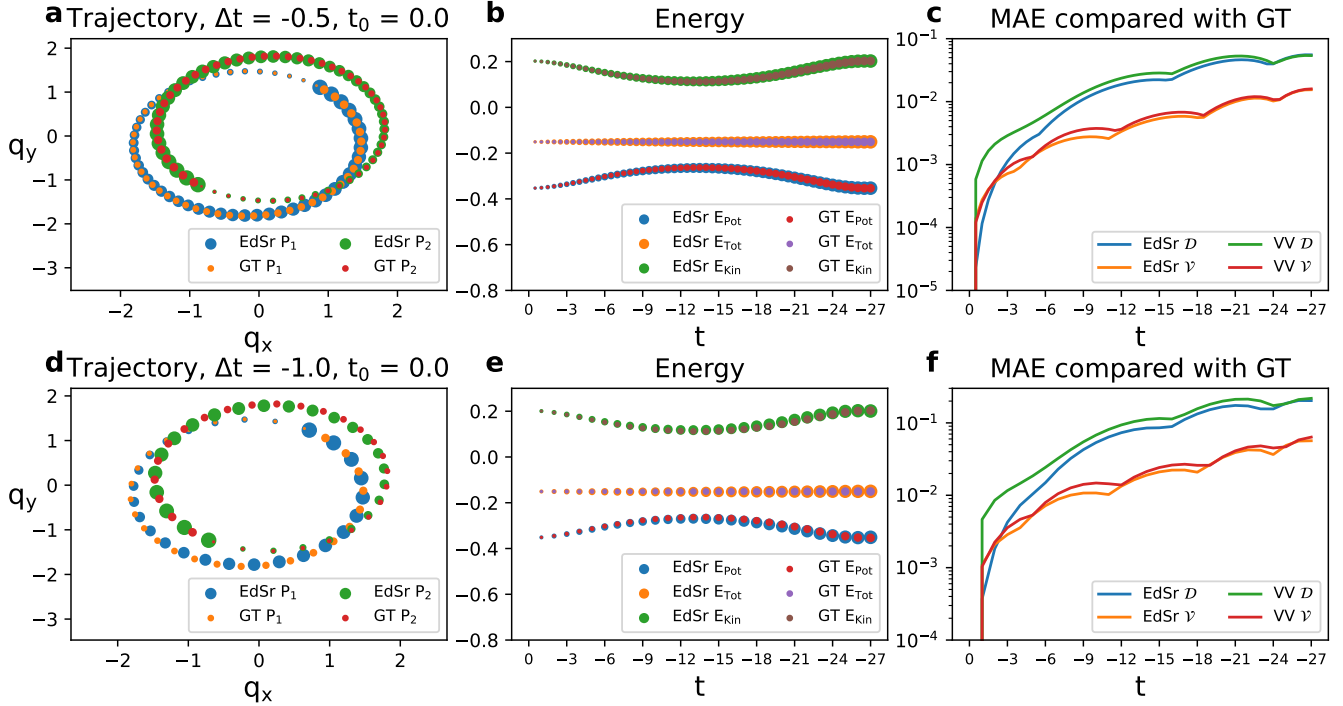


Fig. S7: Results of the second group of sub-experiments of two-body model at different negative Δt . (a), (d) denote the time evolutions of positions of the particles in two-body (P_1 and P_2) generated by EdSr and GT, the symbol sizes increase as the time starts from 0.0 to -27.0. The time evolutions of different energies by EdSr and GT are exhibited in (b), (e). (c), (f) denote the MAEs between EdSr and GT, and compare with those between VV and GT over simulation time.

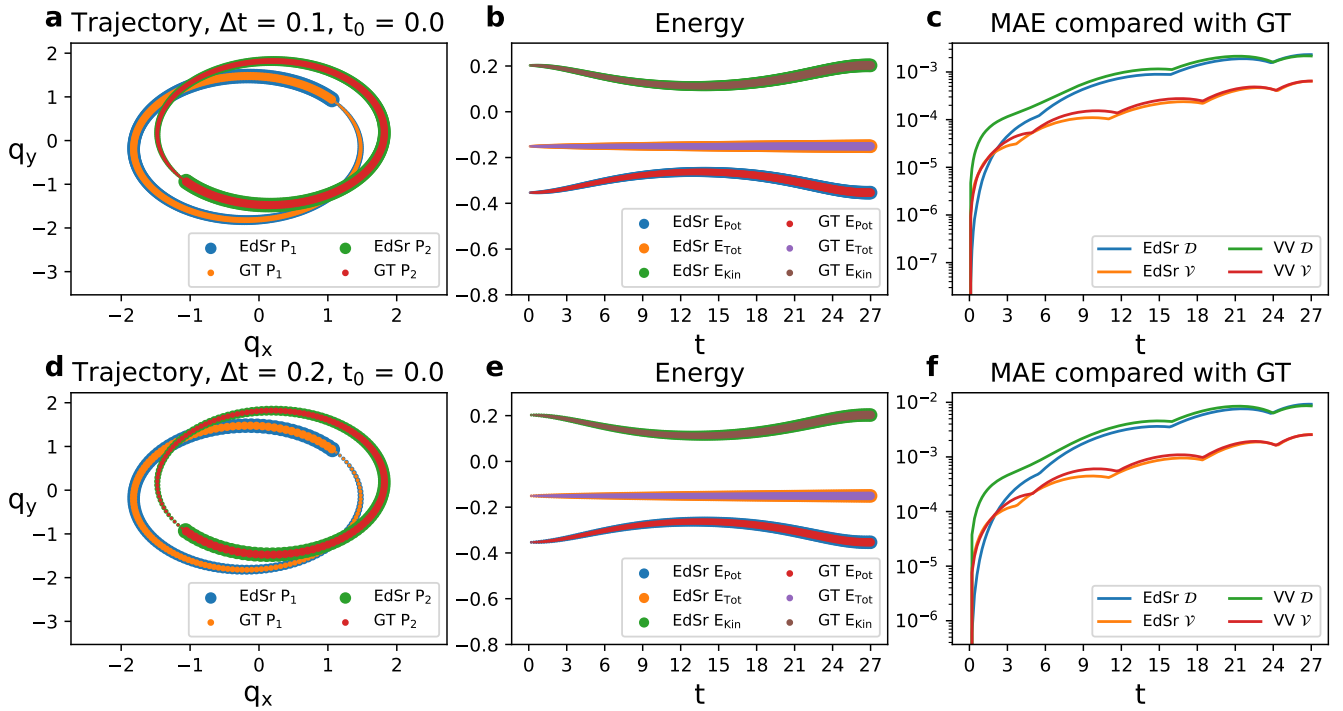


Fig. S8: Results of the second group of sub-experiment of two-body model at $\Delta t = 0.1$ and 0.2 . (a), (d) denote the time evolutions of positions of the particles in two-body (P_1 and P_2) generated by EdSr and GT, the symbol sizes increase as the time starts from 0.0 to 27.0. The time evolutions of energies by EdSr and GT are exhibited in (b), (e). (c), (f) denote the MAEs between EdSr and GT, and compare with those between VV and GT over simulation time.

5 Diffusion of Indole in Zeolite

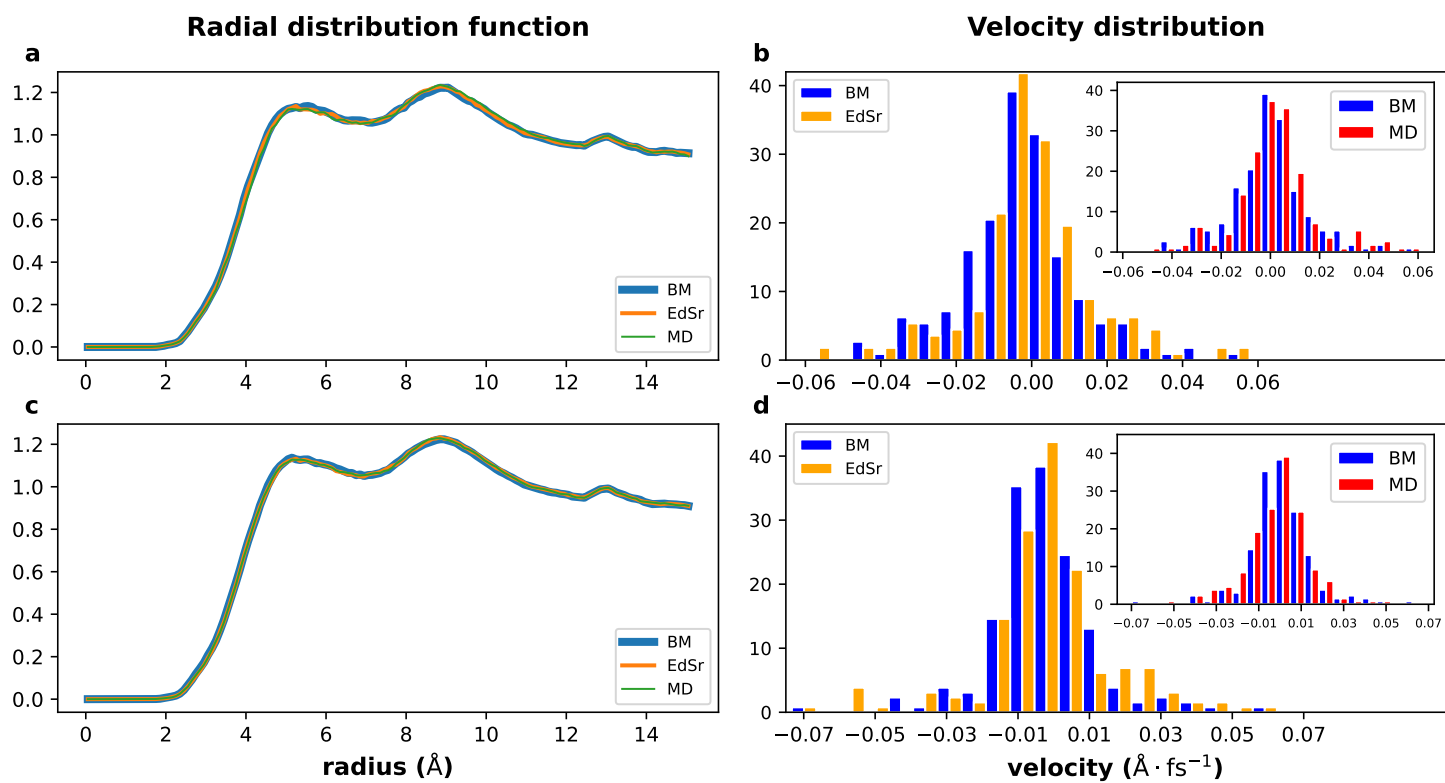


Fig. S9: Radial distribution functions between indole molecules and zeolite (a) and velocity distributions of all indole molecules (b) when the simulations are completed at $\Delta t = 1.0$ fs. (c),(d) show the results at $\Delta t = 3.0$ fs.

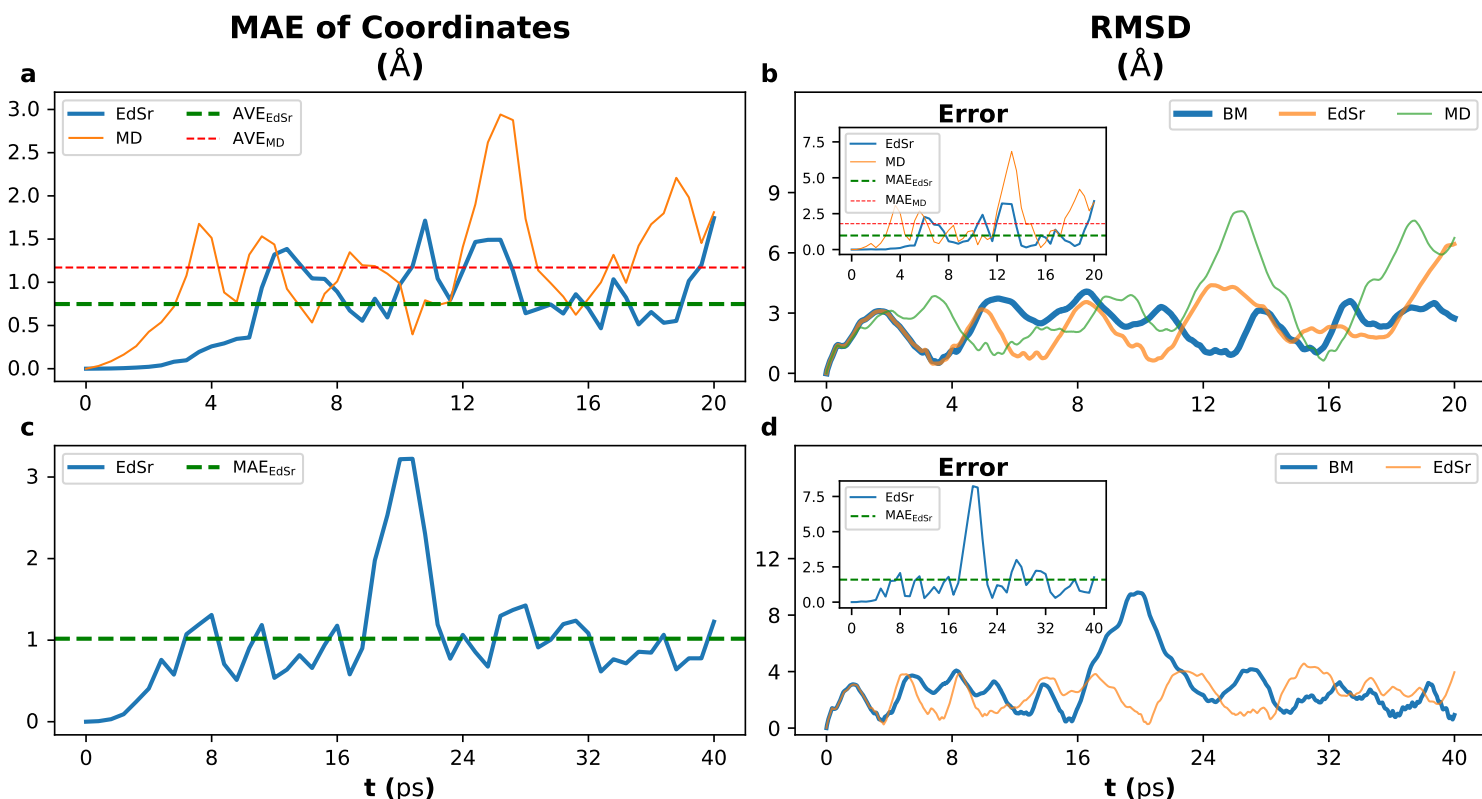


Fig. S10: MAEs between EdSr and BM groups, as well as between VV and BM groups of the atom coordinates of an indole molecule over time at $\Delta t = 2.0$ fs (a) and 4.0 fs (c), the dashed lines in the two sub-figures represent the average MAEs. Time evolutions of RMSDs of BM, EdSr and MD group over time at $\Delta t = 2.0$ fs (b) and 4.0 fs (d), the insets are the AbsVEs, with their MAEs shown as the dashed lines. The results at $\Delta t = 4.0$ fs are the comparison between EdSr and BM groups, as the MD group can not perform at the timestep.

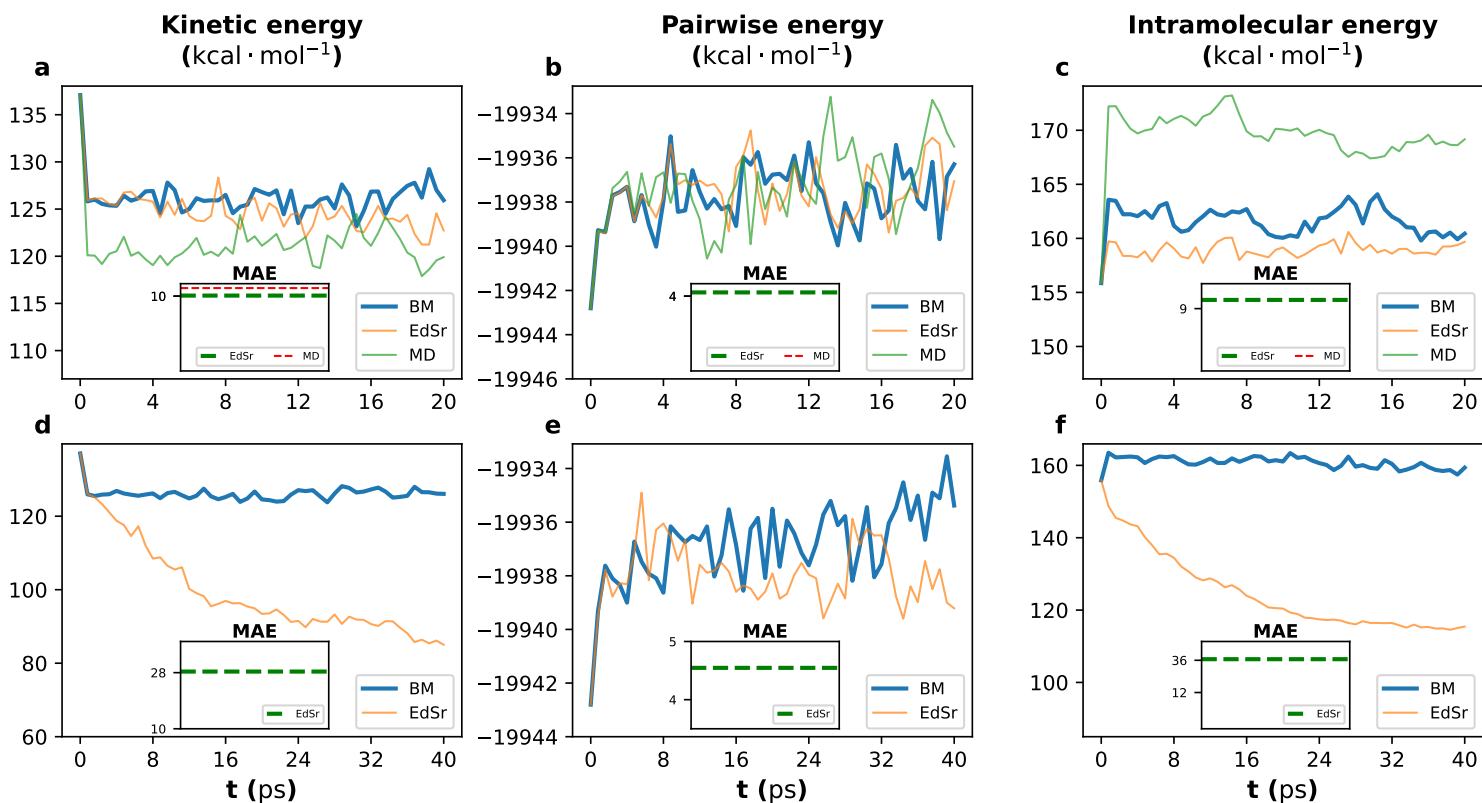


Fig. S11: Time evolutions of different energies obtained by BM, EdSr and MD groups in all-atom MD simulations. (a-c) show the results of $\Delta t = 2.0$ fs, (d-f) show the results of $\Delta t = 4.0$ fs. The MD group can not perform at $\Delta t = 4.0$ fs, so there are no output energies.

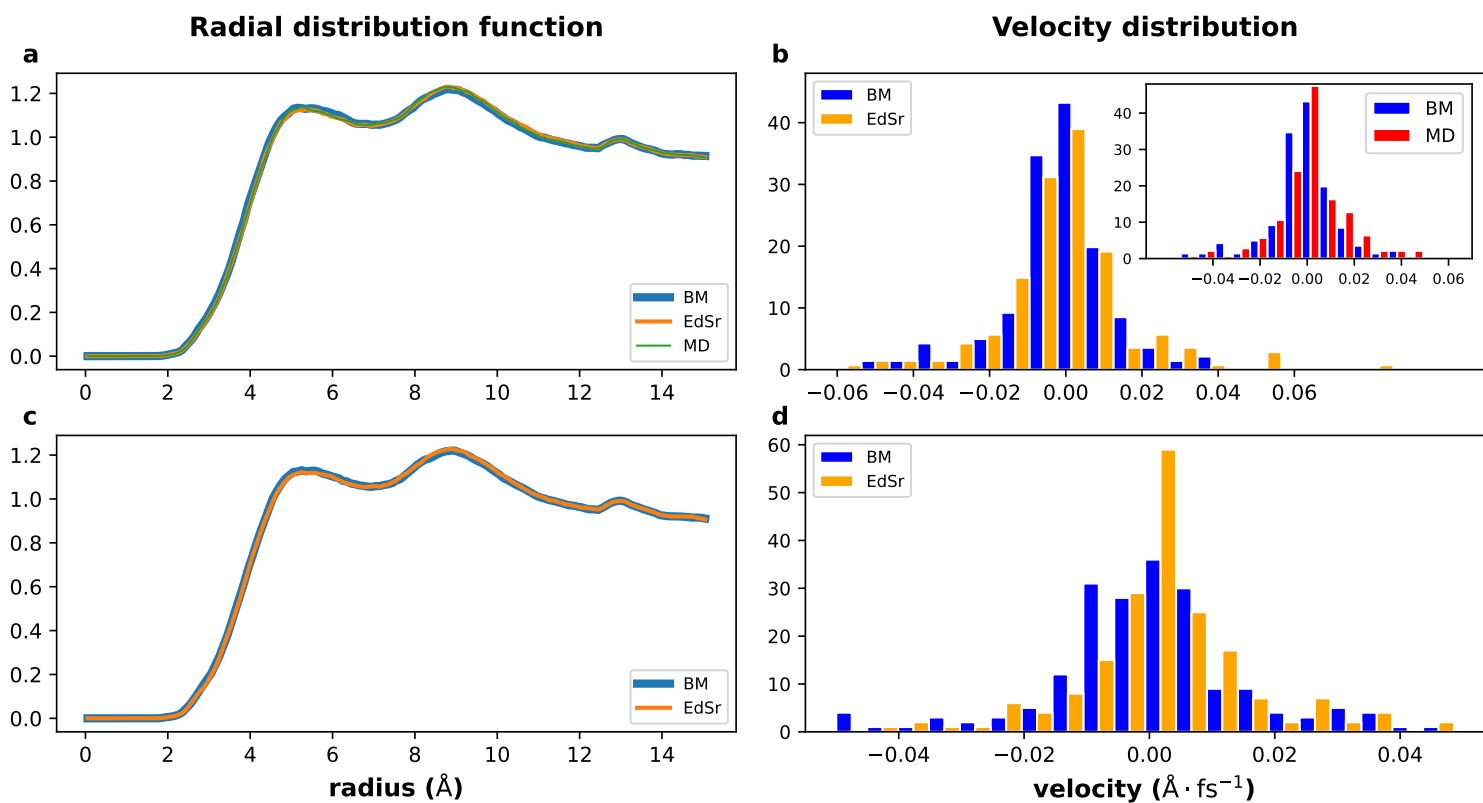


Fig. S12: Radial distribution functions between indole molecules and zeolite (a) and velocity distributions of all indole molecules (b) when the simulations are completed at $\Delta t = 2.0$ fs. (c),(d) show the comparisons between EdSr and BM groups at $\Delta t = 4.0$ fs.

6 Ubiquitin

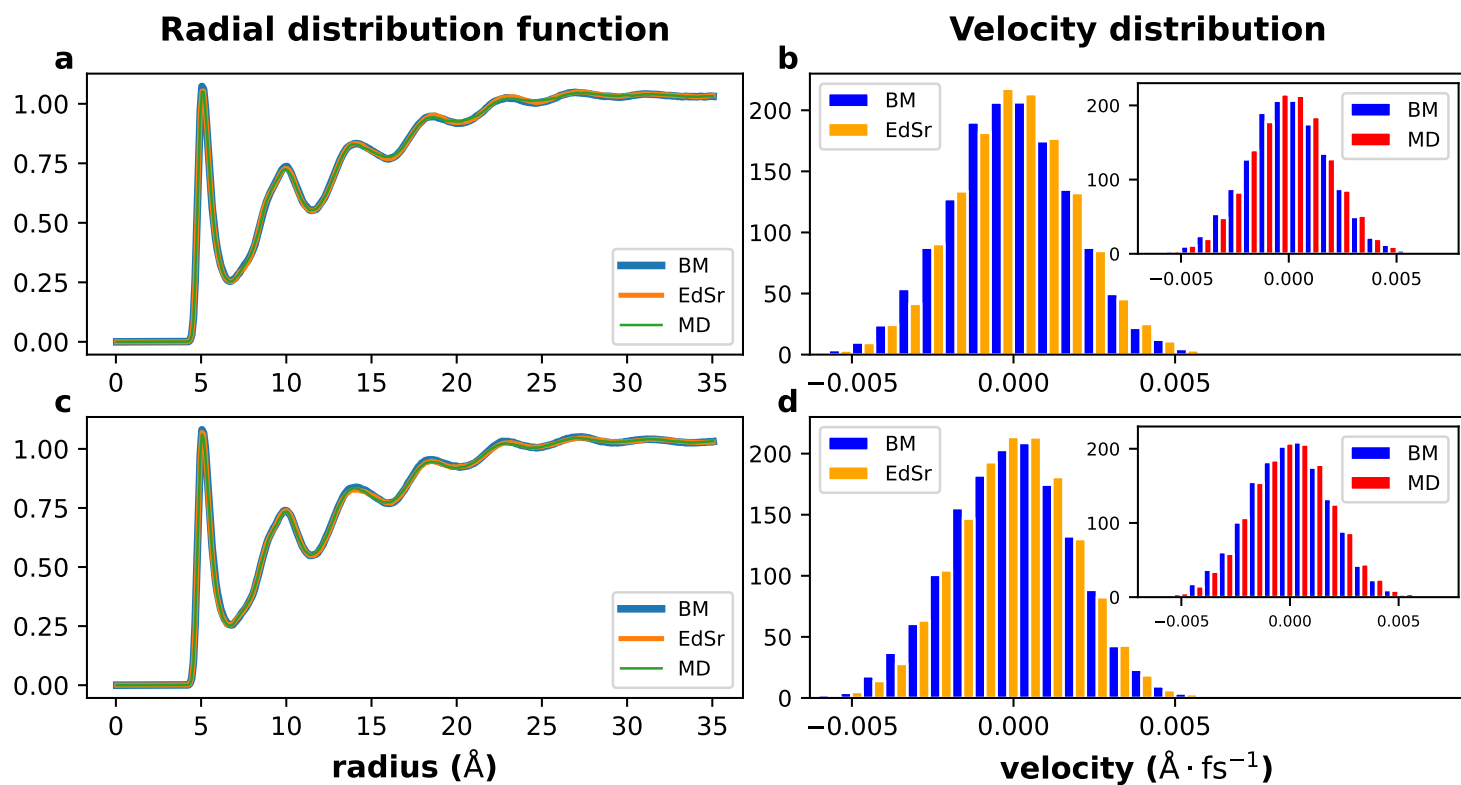


Fig. S13: Radial distribution functions between ubiquitin and water (a) and velocity distributions of all the particles (b) when the BM, EdSr and MD groups are completed at $\Delta t = 10.0$ fs. (c) and (d) show the results at $\Delta t = 20.0$ fs.

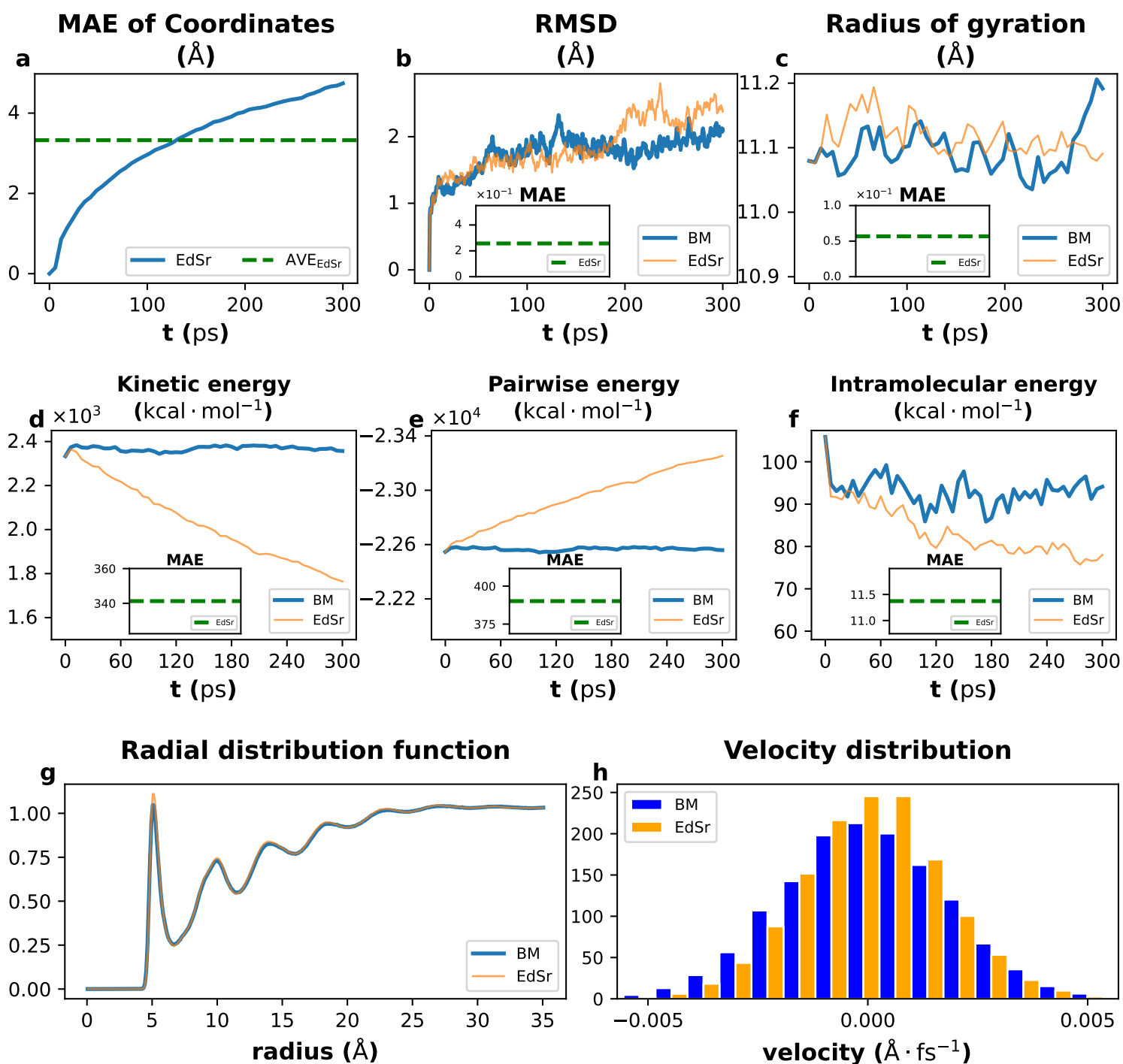


Fig. S14: Results of ubiquitin at $\Delta t = 30.0$ fs by comparing with EdSr and BM groups. The MD group can not perform at such a timestep. (a) shows MAE of coordinates between EdSr and BM. Each point denotes the mean of $3N$ values, where 3 and N denote dimensions, the number of particles in the system, respectively. (b),(c) represent the variation of RMSD, radius of gyration over time, respectively. (d-f) denotes the variations of three kinds of energies over time, the insets are the MAEs of EdSr. (g),(h) show the results of radial distribution functions, and velocity distributions when the simulations complete.

7 Ubiquitin without Water Beads

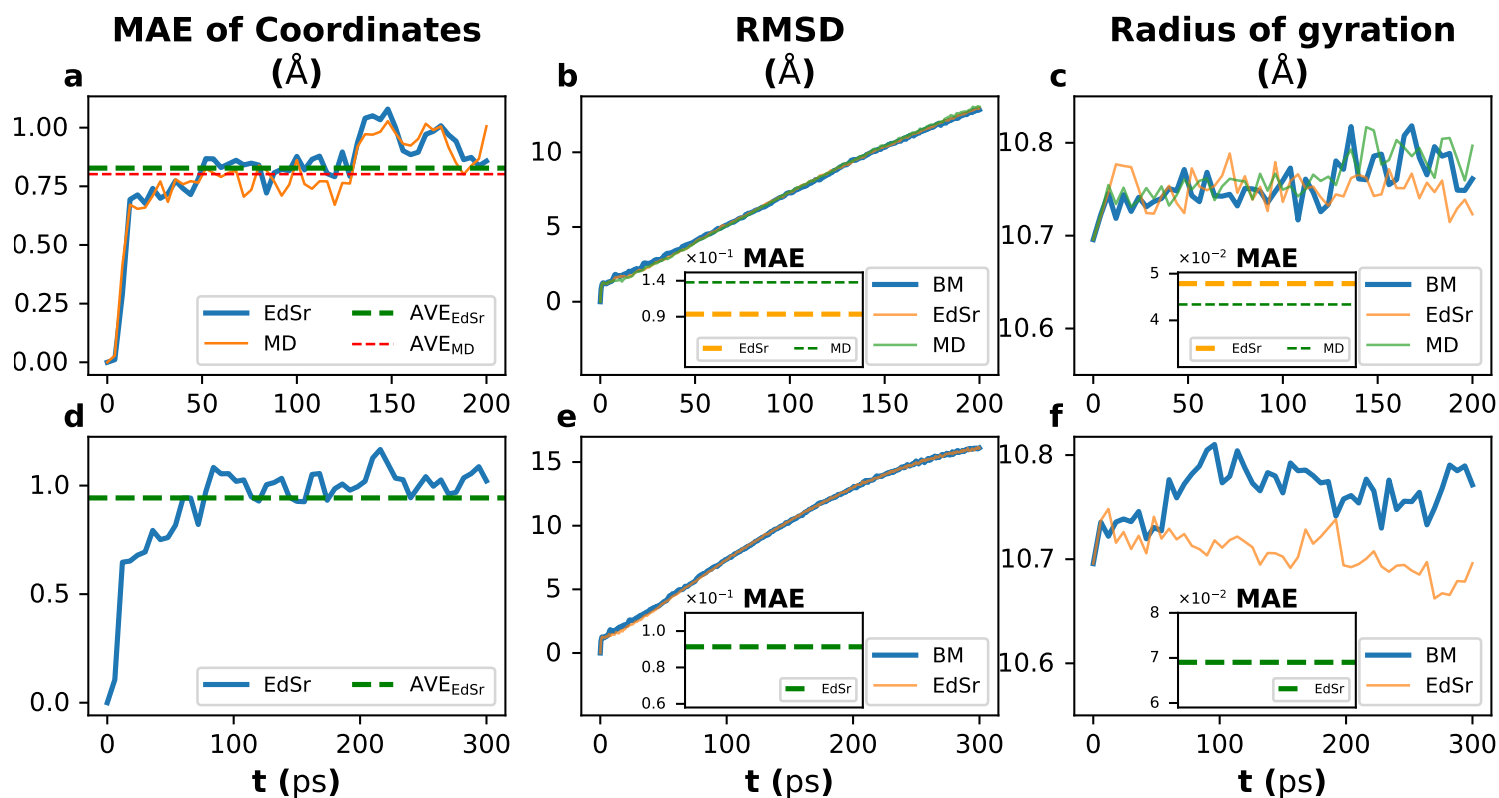


Fig. S15: The comparisons of MAEs of coordinates, RMSDs, radii of gyration obtained via BM, EdSr and MD groups without water beads. (a-c) exhibit the results with $\Delta t = 20.0$ fs. (d-f) exhibit the results with $\Delta t = 30.0$ fs, the MD group can not perform at $\Delta t = 30.0$ fs too.

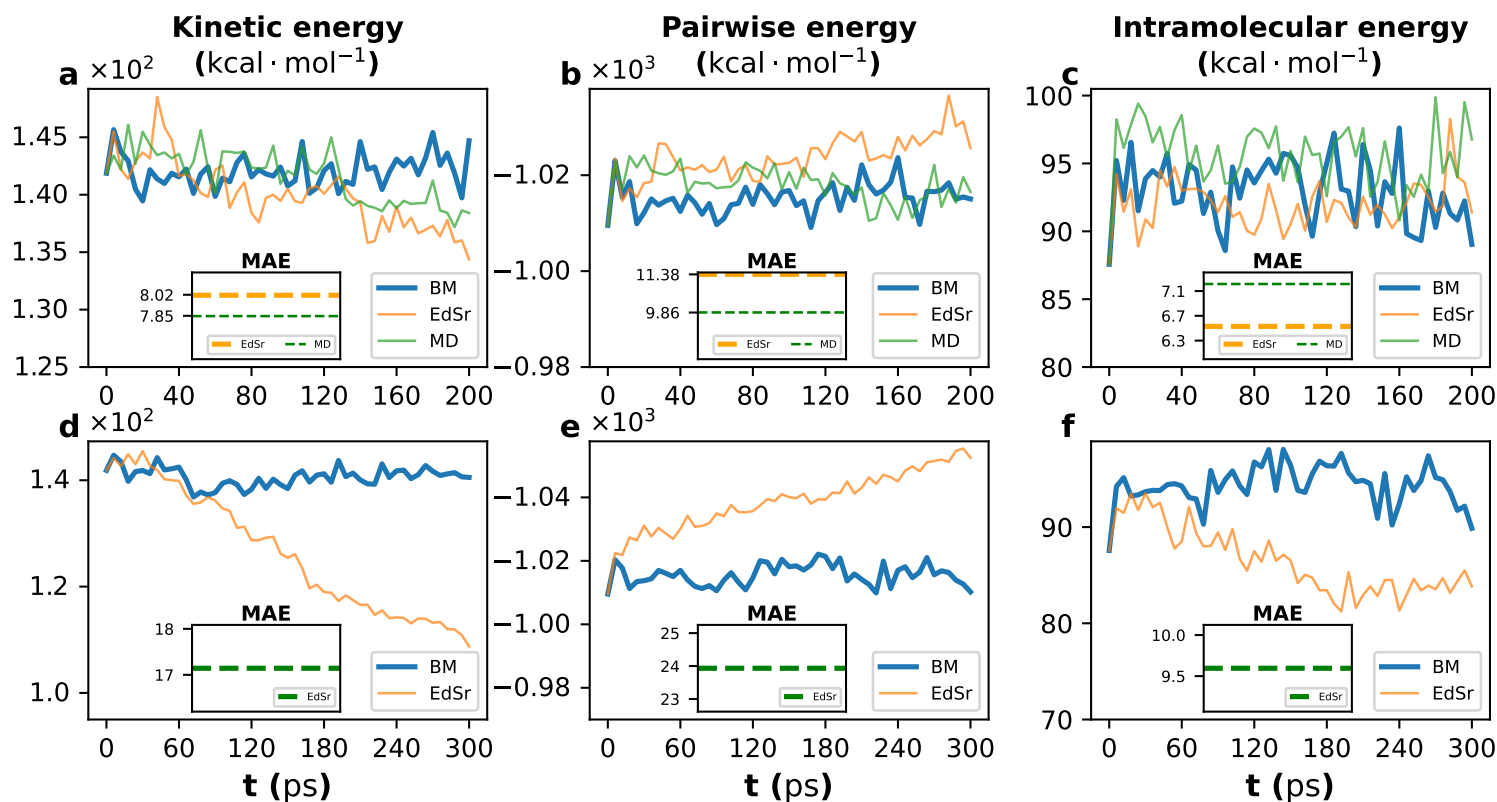


Fig. S16: Time evolutions of kinetic energies, pairwise energies and intramolecular energies obtained via BM, EdSr and MD groups without water beads. (a-c) denote the results with $\Delta t = 20.0$ fs. (d-f) denote the results with $\Delta t = 30.0$ fs.

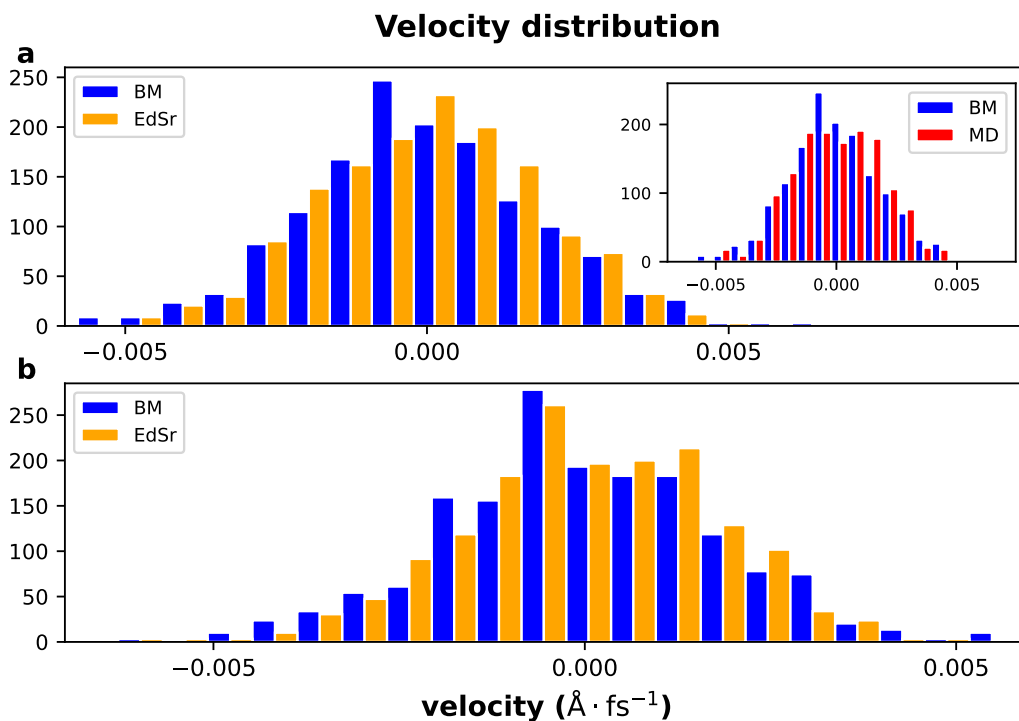


Fig. S17: Velocity distributions of three dimensions when simulations complete. (a) and (b) shown the results at $\Delta t = 20.0$ fs, $\Delta t = 30.0$ fs, respectively.